

AI-guided use of balanced PPAR α / γ dual agonist finetunes macrophage responses in inflammatory bowel disease

Gajanan Katkar

University of California, San Diego

Ibrahim Sayed

University of California, San Diego

Mahitha Shree Anandachar

University of California San Diego

Vanessa Castillo

University of California San Diego

Vidales Eleadah

University of California San Diego

Daniel Toobian

University of California San Diego

Fatima Usmani

University of California San Diego

Joseph Sawires

University of California San Diego

Geoffray Leriche

University of California San Diego

Jerry Yang

University of California, San Diego <https://orcid.org/0000-0002-8423-7376>

William Sandborn

University of California San Diego

Soumita Das

University of California San Diego

Debashis Sahoo

University of California, San Diego <https://orcid.org/0000-0003-2329-8228>

Pradipta Ghosh (✉ prghosh@ucsd.edu)

University of California San Diego

Keywords: Boolean Implication Network, Inflammatory Bowel Disease (IBD), Reactive Oxygen Species (ROS), Macrophage, Bacterial clearance, Citrobacter, PPAR α /g-dual agonists, PAR5359

Posted Date: March 19th, 2021

DOI: <https://doi.org/10.21203/rs.3.rs-243294/v1>

License:  This work is licensed under a Creative Commons Attribution 4.0 International License.

[Read Full License](#)

AI-guided use of balanced PPAR α / γ dual agonist finetunes macrophage responses in inflammatory bowel disease

Authors: Gajanan D. Katkar¹, Ibrahim M. Sayed^{2§}, Mahitha Shree Anandachar², Vanessa Castillo¹, Vidales, Eleadah¹, Daniel Toobian¹, Fatima Usmani², Joseph R. Sawires³, Geoffray Leriche³, Jerry Yang³, William J. Sandborn^{4*}, Soumita Das^{2*}, Debashis Sahoo^{5,6,7*} and Pradipta Ghosh^{1,4,7,8*}

Affiliations:

¹Department of Cellular and Molecular Medicine, University of California San Diego.

²Department of Pathology, University of California San Diego.

³Department of Chemistry and Biochemistry, University of California San Diego

⁴Department of Medicine, University of California San Diego.

⁵Department of Computer Science and Engineering, Jacob's School of Engineering, University of California San Diego.

⁶Department of Pediatrics, University of California San Diego.

⁷Rebecca and John Moore Comprehensive Cancer Center, University of California San Diego.

⁸Veterans Affairs Medical Center, La Jolla, CA.

Alternative affiliation: [§]Department of Medical Microbiology and Immunology, Faculty of Medicine, Assiut University, Egypt.

Conflict of interest statement: S.D, D.S and P.G have a patent on the methodology. Barring this, the authors have declared that no conflict of interest exists.

*Correspondence to:

William J. Sandborn, M.D.; Professor, Department of Medicine, University of California San Diego; 9500 Gilman Drive, MC 0956, La Jolla, CA 92093-0831.

Phone: 858-657-5331, Email: wsandborn@health.ucsd.edu

Soumita Das, Ph.D.; Associate Professor, Department of Pathology, University of California, San Diego; 9500 Gilman Drive, George E. Palade Bldg, Rm 256, 239; La Jolla, CA 92093.

Phone: 858-246-2062 (office): **Email:** sodas@ucsd.edu

Debashis Sahoo, Ph.D.; Assistant Professor, Department of Pediatrics, University of California San Diego; 9500 Gilman Drive, MC 0730, Leightag Building 132; La Jolla, CA 92093-0831.

Phone: 858-246-1803; Fax: 858-246-0019; Email: dsahoo@ucsd.edu

Pradipta Ghosh, M.D.; Professor, Departments of Medicine, and Cell and Molecular Medicine, University of California San Diego; 9500 Gilman Drive (MC 0651), George E. Palade Bldg, Rm 232, 239; La Jolla, CA 92093. Phone: 858-822-7633; Fax: 858-822-7636; Email: prghosh@ucsd.edu

53 **ABSTRACT**

54 A computational platform, the Boolean network explorer (*BoNE*), has recently been developed
55 to infuse AI-enhanced precision into drug discovery; it enables querying and navigating
56 invariant Boolean Implication Networks of disease maps for prioritizing high-value targets.
57 Here we used *BoNE* to query an Inflammatory Bowel Disease (IBD)-map and prioritize two
58 nuclear receptors, PPAR α/γ . Balanced agonism of PPAR α/γ was predicted to impact
59 macrophage processes, ameliorate colitis in network-prioritized animal models, ‘reset’ the gene
60 expression network from disease to health, and achieve a favorable therapeutic index that
61 tracked other FDA-approved targets. Predictions were validated using a balanced and potent
62 PPAR α/γ -dual agonist (PAR5359) in two pre-clinical murine models, i.e., *Citrobacter*
63 *rodentium*-induced infectious colitis and DSS-induced colitis. Mechanistically, we show that
64 such balanced dual agonism promotes bacterial clearance more efficiently than individual
65 agonists both *in vivo* and *in vitro*; PPAR α is required and its agonism is sufficient to induce
66 the pro-inflammatory cytokines and cellular ROS, which are essential for bacterial clearance
67 and immunity, whereas PPAR γ -agonism blunts these responses, delays microbial clearance
68 and induces the anti-inflammatory cytokine, IL10. Balanced agonism achieved controlled
69 inflammation while protecting the gut barrier and ‘reversal’ of the transcriptomic network.
70 Furthermore, dual agonism effectively reversed the defective bacterial clearance observed in
71 PBMCs derived from IBD patients. These findings not only deliver a macrophage modulator
72 for use as barrier-protective therapy in IBD, but also highlight the potential of *BoNE* to
73 accelerate and enhance the precision of drug discovery.

74
75
76

77 **KEY WORDS:**

78 Boolean Implication Network,
79 Inflammatory Bowel Disease (IBD),
80 Reactive Oxygen Species (ROS),
81 Macrophage,
82 Bacterial clearance,
83 *Citrobacter*,
84 PPAR α/γ -dual agonists
85 PAR5359

86

87 INTRODUCTION

88 Inflammatory bowel disease (IBD) is an autoimmune disorder of the gut in which diverse
89 components including microbes, genetics, environment and immune cells interact in elusive
90 ways to culminate in overt diseases¹⁻³. It is also heterogeneous with complex sub-disease
91 phenotypes (i.e., strictures, fistula, abscesses and colitis-associated cancers)^{4,5}. Currently,
92 patients are offered anti-inflammatory agents that have a ~30-40% response-rate, and 40% of
93 responders become refractory to treatment within one year^{6,7}. Little is known to fundamentally
94 tackle the most widely recognized indicator/predictor of disease relapse i.e., a compromised
95 mucosal barrier. Homeostasis within this mucosal barrier is maintained by our innate immune
96 system, and either too little or too much reactivity to invasive commensal or pathogenic
97 bacteria, is associated with IBD⁸. Although defects in the resolution of intestinal inflammation
98 have been attributed to altered monocyte–macrophage processes in IBD, macrophage
99 modulators are yet to emerge as treatment modalities in IBD⁸.

100 We recently developed and validated an AI-guided drug discovery pipeline that uses
101 large transcriptomic datasets (of the human colon) to build a Boolean network of gene clusters
102⁹; this network differs from other computational methods (e.g., Bayesian and Differential
103 Expression Analyses) because gene clusters here are interconnected by directed edges that
104 represent Boolean Implication Relationships that invariably hold true in every dataset within
105 the cohort. Once built, the network is queried using machine learning approaches to identify in
106 an unbiased manner which clusters most effectively distinguish healthy from diseased samples
107 and do so reproducibly across multiple other cohorts (906 human samples, 234 mouse
108 samples). Gene-clusters that maintain the integrity of the mucosal barrier emerged as the genes
109 that are invariably downregulated in IBD, whose pharmacologic augmentation/induction was
110 predicted to ‘reset’ the network. These insights were exploited to prioritize one target,
111 choose appropriate pre-clinical murine models for target validation and design patient-derived
112 organoid models. Treatment efficacy was confirmed in patient-derived organoids using
113 multivariate analyses. This AI-assisted approach provided a first-in-class epithelial barrier-
114 protective agent in IBD and predicted Phase-III success with higher accuracy over traditional
115 approaches⁹.

116 Here we use the same AI-guided drug discovery pipeline, this time to identify and
117 validate a first-in-class macrophage modulator that is predicted to restore mucosal barrier and
118 homeostasis in IBD. We demonstrate the accuracy and predictive power of this network-
119 rationalized approach and reveal the efficacy of balanced dual agonists of PPAR α/γ in two pre-

120 clinical murine models and in patient-derived PBMCs. We also reveal the mechanism(s) of
121 action that enable balanced agonists of this pair of nuclear receptors to reverse some of the
122 fundamental imbalances of the innate immune system in IBD, such that immunity can be
123 achieved without overzealous inflammation.

124 125 **RESULTS** 126

127 **Development of a web-based platform for generating a ‘target report card’**

128 We first developed an interactive, user-friendly web-based platform that allows the querying
129 of our Boolean network-based-IBD map⁹ with just a few intuitive clicks of the mouse, even
130 for biologists (**Supplementary Fig. 1**). With the goal of enabling researchers to pick high-
131 value targets, we programmed the platform to generate a comprehensive automated ‘target
132 report card’ that contains predictions on five components (**Fig. 1A**): (i) *Impact on the outcome*
133 *of IBD in response to treatment*, which shows how levels of expression of any proposed target
134 gene(s) relates to the likelihood of response to therapies across diverse cohorts; (ii) *Therapeutic*
135 *index*, a computationally generated index using Boolean implication statistics which provides
136 a likelihood score of indicate whether pharmacologic manipulation of the target gene(s) would
137 lead to success in Phase III clinical trials; (iii) *Appropriateness of mouse model*, a component
138 that indicates which murine models of colitis shows the most significant change in the target
139 genes (and hence, likely to be best models to test the efficacy of any manipulation of that
140 target); (iv) *Gender bias*, a component that indicates whether the gene is differentially
141 expressed in IBD-afflicted men *versus* women; and (v) *Target tissue/cell type specificity*, which
142 shows the likely cell type where the target is maximally expressed, and hence, the cell type of
143 desirable pharmacologic action. Details of how therapeutic index is computed are outlined in
144 *Methods* and in **Supplementary Fig. 2**; it is essentially a statistical score of how tightly any
145 proposed target gene(s) associates with FDA-approved targets *versus* those that failed.
146 Similarly, details of how cell type of action is computer are outlined in *Methods* and in
147 **Supplementary Fig. 3**.

148
149

150 **PPAR α/γ dual agonists are predicted to be effective barrier-protective agents in IBD**

151 Previous work had identified a little over 900 genes in 3 clusters (Clusters #1-2-3 within the
152 IBD map; **Supplementary Fig. 1A-B**) as potentially high-value targets, all of which were
153 invariably downregulated in IBD-afflicted colons⁹. Reactome analyses showed that epithelial

154 tight junctions (TJs), bioenergetics, and nuclear receptor pathway (PPAR signaling) related
155 genes that are responsible for colon homeostasis are the major cellular processes regulated by
156 these genes (**Supplementary Fig. 1B**). Downregulation of genes in clusters #1-3 was
157 invariably associated also with upregulation of genes in clusters #4-5-6; reactome analyses of
158 the latter showed cellular processes that concern immune cell activation, inflammation and
159 fibrosis, which are hallmarks of IBD (**Supplementary Fig. 1B**). Of the druggable candidates
160 within C#1-2-3, 17 targets were identified as associated with GO biological function of
161 ‘response to stress’/‘response to stimuli’. Targeting one of the 17 targets, PRKAB1, the subunit
162 of the heterotrimeric AMP-kinase engaged in cellular bioenergetics and stress response
163 successfully restored the gut barrier function and also protected it from collapse in response to
164 microbial challenge⁹. Here, we prioritized two more of those 17 targets, PPARA and PPARG,
165 which encode a pair of nuclear receptors, PPAR α and PPAR γ . These two stress/stimuli-
166 responsive genes are equivalent to each other and to PRKAB1, and like PRKAB1, are
167 invariably downregulated in all IBD samples (**Supplementary Fig. 1B-D**). PPARA is in
168 cluster #2 and PPARG is in cluster #3 (**Supplementary Fig. 1B**). They both were located on
169 the two major Boolean paths associated with epithelial barrier and inflammation/fibrosis
170 (**Supplementary Fig. 1B**)⁹. Together, these findings imply three things: (i) that PPARA/G are
171 simultaneously downregulated in IBD, (ii) that such downregulation is invariably associated
172 with inflammation, fibrosis and disruption of the epithelial barrier, and (iii) that simultaneous
173 upregulation of PPARA/G with agonists may restore the gut barrier. The last point is
174 particularly important because PPAR α / γ agonists are known to augment the expression of
175 PPARA/G, and depletion of either reduced the expression of the other¹⁰.

176 Noteworthy, while the role of PPAR γ in colitis has been investigated through numerous
177 studies over the past 3 decades¹¹⁻¹³ (**Table 1**), the role of PPAR α has been contradictory (**Table**
178 **2**), and their dual agonism has never been explored. PPAR γ agonists undeniably ameliorate
179 DSS-induced colitis¹³⁻¹⁵. Although claimed to be effective on diverse cell types in the gut
180 (epithelium, T-cells, and macrophages), the most notable target cells of PPAR γ agonists are
181 macrophages and dendritic cells^{16 17 18 19}. Furthermore, Phase I and II clinical trials with
182 PPAR γ agonists either alone^{20,21} or in combination with mesalamine²² show barrier protective
183 effects in UC patients. Despite these insights, the biopharmaceutical industry has not been able
184 to harness the beneficial impact of this major target within emergent therapeutic strategies
185 largely due to a trail of withdrawals after devastating long-term side effects including heart
186 failure, bone fracture, bladder cancer, fluid retention and weight gain^{23,24}. Intriguingly, and of

187 relevance to this work, the addition of PPAR α -agonistic activity to PPAR γ or δ agonists have
188 led to a higher safety profile, leading to their development for use in many diseases, including
189 type 2 diabetes, dyslipidemia and non-alcoholic fatty liver disease²⁵.

190

191 **An automated target ‘report card’ for PPARA/G in IBD**

192 We next generated an automated target report card for PPARA/G. High levels of both PPARs
193 were sufficient to distinguish healthy from IBD samples, not just in the test cohort that was
194 used to build the IBD-map (ROC AUC of 0.74; **Fig 1B**; see also **Supplementary Fig. 2A-D**),
195 but also in four other independent cohorts with ROC AUC consistently above 0.88 (**Fig 1C**).
196 High levels of both PPARs also separated responders from non-responders receiving TNF α -
197 neutralizing mAbs, GSE16879, E-MTAB-7604 or Vedolizumab that block the $\alpha4\beta7$ integrin
198 to prevent selective gut inflammatory, GSE73661 (ROC AUC 0.63-0.89, **Fig 1D**), inactive
199 disease from active disease (two independent cohorts ROC AUC above 0.93; **Fig 1D**), and
200 quiescent UC that progressed, or not to neoplasia (ROC AUC=1.00 for qUC vs. nUC; **Fig 1D**).
201 High level of PPARA/G was also able to distinguish healthy from diseased samples in diverse
202 murine models of colitis (**Fig 1E**); but such separation was most effectively noted in some
203 models (*Citrobacter* infection-induced colitis, adoptive T-cell transfer, TNBS and *IL10*^{-/-}), but
204 not in others (DSS, and *TNFR1/2*^{-/-}). These findings imply that therapeutics targeting these two
205 genes are best evaluated in the murine models that show the most consistent decrease in the
206 gene expression, e.g., *Citrobacter* infection-induced colitis, adoptive T-cell transfer, TNBS,
207 etc. This was intriguing because the majority (~90%) of the published work on PPARA/G
208 agonists have been carried out in DSS models (**Table 1-2**).

209 The expression profile of the target genes in the gut mucosa revealed that PPARA/G
210 are co-expressed at the highest levels in the crypt top epithelial cells and macrophages (**Fig 1F**;
211 **Supplementary Fig. 3**), predicting that dual agonists are likely to preferentially act on these
212 two cell types. The therapeutic index was below 0.1 for both genes (0.06 for PPARA and 0.04
213 for PPARG; **Fig 1G**; **Supplementary Fig. 2E-F**), aligned well with two other FDA-approved
214 targets shown on the line graph (ITGB1, 0.046 and JAK2, 0.032). The index, which is a
215 statistical measure of the strength of association of PPARA/G with genes that are targets of
216 FDA-approved drugs that have successfully moved through the three phases of drug discovery
217 (i.e., proven efficacy, with acceptable toxicity). A low number is indicative of a high likelihood
218 of success in Phase-III trials. Finally, PPARA/G expression was downregulated to a similar

219 extent in both genders (**Fig 1H**), predicting that therapeutics targeting them are likely to be
220 effective in both men and women.

221

222 **Rationalization of PPARA/G as targets in IBD**

223 Because proteins, but not transcripts, are the targets of therapeutic agents, the impact of
224 therapeutics is translated to cellular processes *via* protein-protein interaction (PPI) networks,
225 a.k.a interactomes. We next asked how dual agonists of PPAR α/γ might impact cellular
226 pathways and processes. A PPI network visualized using PPAR α/γ as ‘query/input’ and the
227 interactive STRING v11.0 database (<https://string-db.org/>) as a web resource of known and
228 predicted protein–protein interactions curated from numerous sources, including experimental
229 data, computational prediction methods and public text collections. PGC1a (a product of the
230 gene PPARGC1A) was a common interactor between the two PPARs (**Fig 2A**). We noted that
231 PGC1a also happens to be a major component within the PPAR α/γ functional network, serving
232 as a central hub for positive feedback loops between the PPARs and their biological function
233 (**Fig 2B**), i.e., mitochondrial biogenesis, DNA replication and energetics (electron transport
234 chain and oxidative phosphorylation). When we analyzed the functional role of the
235 interactomes of PPAR α/γ we noted that indeed both interactomes converged on lipid
236 metabolism, mitochondrial bioenergetics and circadian processes (**Fig 2C**). These findings are
237 consistent with the finding that PPARA/G and PPARGC1A are located within clusters #1-2-3
238 and all of them are predicted to be progressively and simultaneously downregulated in IBD
239 samples (**Fig 2D**; based on the IBD map, **Supplementary Fig. 1**).

240

241 **PPARA/G is downregulated in Ulcerative colitis and Crohn’s Disease**

242 Previous work demonstrated that both PPAR α and PPAR γ are highly expressed in the colon
243 ²⁶. They have also shown that both PPAR α/γ protein and mRNA are downregulated (by ~60%)
244 in active UC and the expression of PPAR γ was significantly associated with disease activity ²⁷.
245 This impaired expression was found in both inflamed and noninflamed areas ²⁸.
246 Polymorphisms have also been detected in PPAR γ ; while some studies found those to be
247 associated with an increased risk for CD ^{29,30}, others found no evidence suggesting any form
248 of association with an increased disease risk ³¹. We collected endoscopically obtained biopsies
249 from the colons of healthy (n = 7) and IBD (n = 14 and 14 of UC and CD, respectively) patients
250 and assessed the levels of transcripts for PPARA/G and PPARGC1A by qPCR (**Fig 2E**). We
251 confirmed that all three transcripts were significantly downregulated in UC and CD samples

252 compared to healthy; both PPARG and PPARGC1a were more significantly downregulated in
253 CD compared to UC (**Fig 2F**). These findings are in keeping with the network-based
254 predictions that these genes should be downregulated invariably in all IBD samples, regardless
255 of disease subtype (see individual disease maps; **Supplementary Fig. 4-5**). While both PPARA
256 and PPARG are in cluster #2 in the UC map, PPARG and PPARA are in separate clusters,
257 clusters 2 and 6, respectively, in the CD map (**Supplementary Fig. 4-5**). Reactome pathway
258 analyses implied that in the case of UC, the two nuclear receptors may co-regulate similar
259 cellular homeostatic processes associated with cluster #2, i.e., mitochondrial biogenesis and
260 translation initiation, infectious disease and detoxification of ROS (see **Supplementary Fig.**
261 **4**). By contrast, in the case of CD, they may independently regulate diverse cellular processes
262 that maintain cellular homeostasis; while PPARG is associated with cellular metabolism (TCA
263 cycle) and inhibition of NFkB signaling, PPARA is associated with transcriptional activity of
264 nuclear receptors, cholesterol biosynthesis and Met/Ras signaling (see **Supplementary Fig.**
265 **5**). Taken together, these findings demonstrate that both targets are downregulated in IBD and
266 that they may regulate key pathophysiologic processes that are vital for cellular homeostasis.

267

268 **Synthesis and validation of PAR5359, a potent and specific PPAR α/γ dual agonist**

269 We noted that all commercially available PPAR α/γ dual agonists lack ‘balanced’ agonistic
270 activities (**Table 3**)^{32,33}. Drugs that have fallen aside due to safety concerns also lack balanced
271 agonism; most of them are more potent on PPAR γ than on PPAR α by a log-fold (**Table 3**). All
272 these PPAR α/γ dual agonists have been withdrawn due to safety concerns²⁵, but the cause of
273 the ‘unsafe’ profile remains poorly understood. Saroglitazar, the drug that is the only active
274 ongoing Phase-III trial (NCT03061721) in this class, has ~3 log-fold more potency on PPAR α
275 than PPAR γ ³⁴. Because our AI-guided approach suggested the use of simultaneous and
276 balanced agonism, we favored the use of the only balanced and yet, specific PPAR α/γ agonist
277 described to date, PAR5359^{35,36} (see **Table 4**). In the absence of commercial sources or well-
278 defined methods on how to synthesize this molecule, we generated PAR5359 in 4 synthetic steps
279 (see details in *Methods*) and confirmed its specificity and the comparable agonistic activities
280 using pure single PPAR α [GW7647³⁷] or PPAR γ [Pioglitazone³⁸] agonists as controls
281 (**Supplementary Fig. 6**). With these potent and specific compounds as tools, and their doses
282 adjusted to achieve the same potency, we set out to validate the network-based predictions
283 using pre-clinical models.

284

285 **PAR5359 ameliorates *C. rodentium*-induced colitis, enhances bacterial clearance**

286 We next sought to assess the efficacy of individual and dual agonists of our compounds in
287 murine pre-clinical models. PPAR α/γ 's role (or the role of their agonists) in protecting the gut
288 barrier has been evaluated primarily in DSS-induced colitis (**Table 1, 2**). However, *BoNE*
289 prioritized other models over DSS, many of which accurately recapitulate the
290 PPAR α/γ -downregulation that is observed in the barrier-defect transcript signature in human
291 IBD (**Fig. 1E**). Among those, we chose *C. rodentium*-induced infectious colitis, a robust model
292 to study mucosal immune responses in the gut and understand derailed host-pathogen
293 interaction in IBD³⁹⁻⁴¹. Furthermore, this model requires the balanced action of macrophages
294 (a cell line predicted to be the preferred cell type target; **Fig. 1F**) to promote bacterial clearance
295 and healing⁴².

296 Colitis was induced by oral gavage of *C. rodentium* and mice were treated daily with
297 the drugs *via* the intraperitoneal route (see workflow detailed in **Fig. 3A, Supplementary Fig.**
298 **7A**). The dose for each drug was chosen based on their *EC*₅₀ on their respective targets so as
299 to achieve equipotent agonistic activities (**Supplementary Fig. 6**). Fecal pellets of individual
300 mice were collected to determine the number of live bacteria present in the stool. As
301 anticipated, the bacterial burden in all mice increased from day 5, reaching a peak on day 7,
302 forming a plateau until day 11 before returning to pre-infection baseline by day 18 (**Fig. 3B**).
303 Compared against all other conditions, PAR5359-treated mice cleared the gut bacterial load
304 significantly and rapidly (**Fig. 3B-D**). *Citrobacter* infection was associated with significant
305 epithelial damage and profuse infiltration of inflammatory cells and edema by day 7
306 (**Supplementary Fig. 7B**) most of which resolved by day 18 (DMSO control; **Fig. 3E**). Colons
307 collected on day 7 showed that treatment with PAR5359 significantly reduced these findings
308 when compared to vehicle (DMSO), PPAR α and PPAR γ agonists alone (**Supplementary Fig.**
309 **7B**). Unexpectedly, when we analyzed the colons on day 18, we noted persistent immune
310 infiltrates in tissues in two treatment arms, pioglitazone and GW7647 (arrowheads; **Fig. 3E**),
311 but not in the vehicle control group, or those treated with PAR5359. These findings indicate
312 that individual PPAR α or PPAR γ agonists may either retard bacterial clearance and/or induce
313 an overzealous amount of inflammation, but the balanced dual agonist (PAR5359) may have
314 effectively cleared infection and resolved inflammation. PAR5359 also reduced spleen
315 inflammation as evidenced by a decreased spleen weight and length compared to vehicle
316 control (**Supplementary Fig. 7C-F**). The spleens of mice treated with DMSO, PPAR α -alone
317 agonist, GW7647 and PPAR γ -alone agonist, Pioglitazone showed black-discoloration,

318 presumably infarcts (arrows, **Supplementary Fig. 7C, 7E**). Notably, the spleens of mice
319 treated with PPAR α -alone agonist, GW7647, showed a significant increase in spleen length
320 (**Supplementary Fig. 7D, 7F**).

321 Taken together, these findings indicate that PPAR α/γ dual agonist PAR5359 is superior
322 in ameliorating *C. rodentium*-induced colitis than either PPAR α or PPAR γ agonist used alone.
323 Treatment with the dual, but not the single agonists hastened bacterial clearance, resolved
324 inflammation, and induced healing.

325

326 **PAR5359 resists *C. rodentium*-induced gene expression changes in the colon**

327 We next sought to determine if pharmacologic augmentation of PPARA/G was sufficient to
328 influence the entire transcriptomic network *via* the invariant Boolean implication relationships
329 between the gene clusters. RNA sequencing (RNA-seq) studies were carried out on the *C.*
330 *rodentium*-infected colons in each treatment group (**Fig. 3A**). As expected, downregulation of
331 genes in clusters #1-2-3 of the IBD-map was significant in infected (DMSO) vs uninfected
332 controls, indicative of network shift from health towards disease (**Fig. 3F**); PAR5359-treatment
333 resisted such shift.

334 Pre-ranked gene set enrichment analyses (GSEA) based on pair-wise differential
335 expression analysis showed that when compared to DMSO control, dual PPAR α/γ agonism
336 with PAR5359, but not individual agonists Pioglitazone or GW7647 was able to significantly
337 preserve epithelial junction signatures (both tight and adherens junctions) and balance
338 macrophage processes (compare **Fig. 3G** with **Supplementary Fig. 8A**). These findings are in
339 keeping with the predictions that epithelial cells and macrophages maybe the primary cell type
340 of action for dual PPAR α/γ agonists. Comparison of all treatment cohorts against each other
341 revealed that although both PAR5359 and Pioglitazone were superior to GW7647 in
342 maintaining some epithelial processes (differentiation, tight junctions) and macrophage
343 processes (**Supplementary Fig. 8B-E**), PAR5359 emerged as the only group that maintained
344 homeostatic PPAR signaling in nature and extent as uninfected control (**Supplementary Fig.**
345 **8F**).

346 Taken together, these findings suggest that dual agonists of PPAR α/γ are sufficient to
347 either resist network shift and/or reverse the disease network in the setting of colitis. They also
348 offer clues suggestive of epithelial and macrophage processes, two key cellular components of
349 innate immunity in the gut lining as major mechanisms. These transcriptome wide impacts

350 suggest that PPAR α / γ dual agonist PAR5359 is superior in restoring colon homeostasis in *C.*
351 *rodentium*-induced colitis than either PPAR α or PPAR γ agonist used alone.

352

353 **PAR5359 ameliorates DSS-induced colitis**

354 It is well known that no single mouse model recapitulates *all* the multifaceted complexities of
355 IBD^{43,44}. Because almost all studies evaluating PPAR α / γ -modulators have been performed on
356 the DSS-induced colitis model (**Table 1-2**), we asked whether the PPAR α / γ dual agonist
357 PAR5359 can ameliorate colitis in this model. Mice receive intrarectal DMSO vehicle control
358 or PAR5359 while receiving DSS in their drinking water (**Supplementary Fig. 9A**). Disease
359 severity parameters, i.e., weight loss, disease activity index, shortening of the colon and histology
360 score were significantly ameliorated in the PAR5359-treated group (**Supplementary Fig. 9A-E**).
361 These findings show that the PPAR α / γ -dual agonist, PAR5359, is also effective in DSS-
362 induced colitis. It is noteworthy that the PAR5359 dual agonist offered protection in the DSS-
363 model, because prior studies using the same model have demonstrated that PPAR α -agonists
364 worsen^{45,46}, and that the PPAR γ -agonists ameliorate colitis⁴⁷⁻⁴⁹ (see **Table 1-2**).

365

366 **PAR5359 promotes bacterial clearance with controlled production of ROS and** 367 **inflammation in peritoneal macrophages**

368 Because the intestinal macrophages play a crucial role in maintaining the integrity of the gut
369 epithelial barrier and in the control of pathogen invasion by triggering an appropriate immune
370 response, the fine-tuning macrophage is essential in maintaining homeostasis and, potentially,
371 the development of IBD. To explore the mechanism(s) by which dual, but not individual, PPAR
372 agonists may alter macrophage response to microbes, we incubated macrophages treated or not
373 with the drugs and challenged them with CD-associated adherent invasive *E. coli* (*AIEC*)-
374 *LF82*; this strain, originally isolated from a chronic ileal lesion from a CD patient⁵⁰. As for the
375 source of macrophages, we isolated metabolically active primary murine peritoneal
376 macrophages using Brewer thioglycolate medium using established protocols^{51,52}. These
377 macrophages are known to have high phagocytic activity⁵¹ (**Fig. 4A**). Thioglycolate-induced
378 peritoneal macrophages (TG-PMs) were lysed, and viable intracellular bacteria were counted
379 after plating on an agar plate. Pre-treatment with 1 μ M PAR5359 and an equipotent amount of
380 GW7647 (PPAR α agonist) promoted bacterial clearance and reduced the bacterial burden
381 when compared to vehicle control (**Fig. 4B**). By contrast, pre-treatment with Pioglitazone
382 (PPAR γ agonist) inhibited bacterial clearance; notably, bacterial burden was significantly

383 higher at both 3 h and 6 h after infection (**Fig. 4B**). Reduced clearance of microbes in the latter
384 was associated also with reduced cellular levels of reactive oxygen species (ROS) (**Fig. 4C**);
385 oxidative burst and induction of ROS is key component for effective bacterial killing^{53,54}.
386 PAR5359 did not interfere with the production of microbe-induced ROS, and the PPAR α
387 agonist (GW7647) was permissive to ROS induction (in fact, even induces it over bacteria-
388 alone control) during initial time points after infection (**Fig. 4C**).

389 These patterns of microbial clearance and cellular ROS were associated also with the
390 expression of cytokines, as determined by qRT-PCR analyses (**Fig. 4D**). As expected, infection
391 of TG-PM with *AIEC*-LF82 induced *il1 β* , *il6*, *tnf α* and *il10*. PAR5359 significantly and
392 selectively suppressed the expression of the pro-inflammatory cytokines *il1 β* , *il6* and *tnf α* (but
393 not the anti-inflammatory cytokine, *il10*) (**Fig. 4D**). By contrast, the PPAR γ -specific agonist
394 pioglitazone significantly and indiscriminately suppressed all the cytokines, while there was
395 no effect of the PPAR α specific agonist GW7647 (**Fig. 4D**). ELISA studied on the supernatant
396 media further confirmed these findings (**Fig. 4E**), demonstrating that the effects in gene
397 expression were also translated to the levels of secreted cytokine protein released by the
398 macrophages in the supernatant.

399 It is noteworthy that for the most part, the qPCR (**Fig. 4D**) and ELISA (**Fig. 4E**) studies
400 matched, except *il10*; although pioglitazone appeared to suppress *il10* mRNA, it did not
401 suppress the levels of the *il10* protein, suggesting that PPAR γ -agonist is sufficient for an overall
402 anti-inflammatory phenotype. Similarly, although GW7647 appeared to not affect *il10* mRNA,
403 it suppressed the levels of the *il10* protein, suggesting that PPAR α agonist is sufficient for an
404 overall pro-inflammatory phenotype. Similar findings were also observed in the case of another
405 enteric pathogen, *S. enterica*, i.e., unlike the dual agonist, neither PPAR α nor PPAR γ agonist
406 could enhance bacterial clearance with a modest induction of pro-inflammatory cytokines
407 (significantly lower than control) and, yet, had no impact on anti-inflammatory IL10
408 production (**Supplementary Fig. 10**).

409 Taken together, these results show that- (i) PPAR γ -agonism induces ‘tolerance’ by
410 suppressing inflammation, inhibiting ROS production and delaying bacterial clearance; (ii)
411 PPAR α -agonism enhances the induction of inflammation and ROS, and promotes bacterial
412 clearance; and (iii) PPAR α/γ -dual agonism strikes a somewhat balanced response. The latter
413 suppresses proinflammatory cytokines without suppressing anti-inflammatory cytokine *il10*,
414 and is permissive to inflammation and ROS induction that is optimal and sufficient to promote
415 bacterial clearance.

416 **PPAR α , but not PPAR γ is required for the induction of inflammatory cytokines and ROS**

417 To further dissect which nuclear receptors are responsible for the balanced actions of the dual
418 agonist, we next used a set of highly specific and potent PPAR α / γ -inhibitors (**Table 4**). We
419 pre-treated TG-PMs with PPAR α and PPAR γ inhibitors, either alone, or in combination,
420 followed by stimulation with bacterial cell wall component LPS (**Fig. 5A**). As expected, LPS
421 induced the cellular levels of ROS (**Fig. 5B**) and inflammatory cytokines (**Fig. 5C-D**) in TG-
422 PMs significantly higher than in untreated control cells. Inhibition of PPAR α suppressed the
423 induction of cellular ROS and inflammatory cytokines, both at the level of gene and protein
424 levels (**Fig. 5B-D**). By contrast, inhibition of PPAR γ did not interfere with either response (**Fig.**
425 **5B-D**). Simultaneous inhibition of both PPAR α and PPAR γ mimicked the cellular phenotypes
426 in the presence of PPAR α -inhibitors (**Fig. 5B-D**), indicating that inhibition of PPAR α is
427 sufficient to recapitulate the phenotype of dual inhibition. Taken together, these findings
428 indicate that PPAR α is required for the proinflammatory response of macrophages.

429

430 **PPAR α / γ dual agonist PAR5359 promotes bacterial clearance in patient-derived PBMCs**

431 In search of a pre-clinical human model for testing drug efficacy, we next assessed microbial
432 handling by PBMCs derived from patients with IBD and compared them with that in age-
433 matched healthy volunteers. We enrolled both male and female patients and both CD and UC
434 (**Table 5**). Consecutive patients presenting for routine care to the UC San Diego IBD clinic
435 were enrolled into the study; the only exclusion criteria were failure to obtain informed consent
436 for the study or active infections and/or disease flare. Peripheral blood collected in the clinic
437 was freshly processed as outlined in **Fig. 6A** to isolate PBMCs. Pre-treatment for 30 min with
438 vehicle or PAR5359 was followed by infection for 1h. Subsequently, the cells were treated
439 with gentamicin for 60 min to kill extracellular bacteria to assess intracellular bacterial burden
440 at 1 and 6 h after the gentamicin wash.

441 Two observations were made: *First*, CD but not UC patient-derived PBMCs when
442 infected with *AIEC*-LF82 showed an increased number of internalized viable bacteria when
443 compared to healthy PBMCs (**Fig. 6B, 6E**), indicative of either defective clearance and/or
444 increased permissiveness to bacterial replication within the cells is limited to the CD. *Second*,
445 pre-treatment with PAR5359 could improve clearance significantly (**Fig. 6C-D, 6F-G**). These
446 results indicate that bacterial clearance is delayed in PBMCs of patients with CD and that
447 PPAR α / γ dual agonism with PAR5359 can reverse that defect. The possibility that such
448 reversal could be due to any direct bacteriostatic/-cidal effect of PAR5359 agonist was ruled

449 out (see bacterial viability assay in **Supplemental Fig. 11**). Our findings demonstrate that
450 bacterial clearance is delayed primarily in CD and not UC are in keeping with the fact that
451 delayed bacterial clearance from inflamed tissues (up to ~4-fold) is uniquely observed in CD
452 ⁵⁵. These findings are also in keeping with our own observation that the downregulation of
453 PPARG/PPARGC1A was more prominent in patients with CD (**Fig. 2E-F**). In fact, delayed
454 clearance is one of the major reasons for persistent inflammation and disease progression
455 among patients with CD ^{55,56}.

456

457 **DISCUSSION**

458 Barrier-protection/restoration is the treatment endpoint for all clinical trials in IBD
459 therapeutics; however, despite much success in the development of anti-inflammatory
460 therapies ^{7,57}, barrier-protective therapeutics in IBD have been slow to emerge ⁵⁸. Here we
461 report the discovery of an effective barrier-protective therapeutic strategy in IBD identified
462 using an AI-guided navigation framework (summarized in **Fig 7**). *First*, a network-based drug
463 discovery approach ⁹ was used to identify, rationalize and validate dual and balanced agonism
464 of PPAR α/γ (but not one at a time) is necessary for therapeutic success. *Second*, we provided
465 evidence in the form of proof-of-concept studies (in two different pre-clinical murine models)
466 demonstrating that the simultaneous and balanced agonistic activation of the pair of PPARs as
467 an effective barrier protective strategy in IBD. *Third*, we demonstrate that macrophages are
468 one of the primary target cell type of this therapeutic strategy; dual agonist (but not single) was
469 permissive to the induction of macrophage responses expected for optimal immunity without
470 overzealous inflammation. There are *three* notable takeaways from this study, which are
471 unexpected observations and/or insights that fill key knowledge gaps in the fields of – (a)
472 network medicine, (b) IBD therapeutics and (c) macrophage biology.

473 *First*, with regard to network medicine, the AI-guided approach we used here differs
474 from the current practice in three fundamental ways: 1) Unlike most studies that prioritize
475 targets based on Differential Expression Analysis (DEA, or integrated DEA) or Bayesian
476 approaches, target identification and prediction, this work was guided by a Boolean implication
477 network of continuum states in *human* disease ⁹; 2) Instead of conventional approaches of trial-
478 and-error, intuitive guess and/or knowledge-based prioritization of study models (animal or
479 cell-type of action), target validation in network-rationalized animal and cell-type models that
480 most accurately recapitulate the role of the target(s) during disease progression; 3) Inclusion of
481 human pre-clinical model (patient-derived PBMCs) for target validation, inspiring the concept
482 of *Phase '0' trials* that have the potential to personalize the choice of therapies. The combined

483 synergy of these approaches validates a first-in-class macrophage modulator in addressing the
484 broken gut barrier in IBD.

485 The impact of using such an approach is 4-fold: (i) Because the network approach used
486 here relies on the fundamental invariant Boolean implication relationships between genes, and
487 their patterns of changes in expression between healthy and IBD samples, such ‘rule of
488 invariant’ implies that any given relationship and/or change in expression pattern annotated
489 within the network *must* be fulfilled in every IBD patient. By that token, targets/drugs
490 prioritized based on this network is expected to retain efficacy beyond inbred laboratory mice,
491 into the heterogeneous patient cohorts in the clinic. (ii) This AI-guided approach not just helped
492 compute pre-test probabilities of success (“*Therapeutic Index*”), but also helped pick models
493 that are most insightful and appropriate to demonstrate therapeutic efficacy (e.g., *Citrobacter*
494 *rodentium* infection-induced colitis) and to pinpoint the cell type and mechanism of action
495 (microbial clearance by macrophages). This is noteworthy because the conventional approach
496 in studying PPARs has been limited to the use of DSS-induced colitis (see **Table 1-2**), which
497 has often given conflicting results (see **Table 2**). In fact, without the use of the *Citrobacter*
498 *rodentium* infectious colitis model, the deleterious effects of PPAR γ agonists would have been
499 overlooked. (iii) Having a computational framework improves precision in target
500 identification; it is because of the emergence of the two PPARs (alongside their positive
501 feedback regulator, PGC1a) within our network, we rationalized their dual agonism as a
502 preferred strategy (over single) and our experiments validated that prediction both *in vivo* and
503 *in vitro*. This is noteworthy because conventional approaches have demonstrated a protective
504 role of PPAR γ agonists and a conflicting (both protective and exacerbating) role of PPAR α in
505 IBD^{46,59-61}; the advantage of dual agonism has neither been rationalized nor tested. (iv) The
506 ‘target report card’, like the one shown here, is a project navigation tool that is geared to
507 streamline decision-making (i.e., which genes, which animal models, which cell type/cellular
508 process, what is the likelihood of success, etc.), which in turn should reduce attrition rates,
509 waste and delays; the latter are well-recognized flaws in the current process of drug discovery.

510 *Second*, regarding IBD therapeutics, our studies demonstrate that single or unbalanced
511 combinations of PPAR agonists are inferior to dual/balanced agonists. Conventional and
512 reductionist approaches have inspired numerous studies with single PPAR agonists over the
513 past decade (**Tables 1-2**). However, given the devastating side effects of most single or
514 unbalanced PPAR α/γ agonists (**Table 3**), translating to the clinic beyond a Phase II trial^{20,62,63}
515 has not been realized. Because the therapeutic index for the dual PPAR α/γ agonists matches

516 that of other FDA-approved targets/drugs, it is predicted that barring unexpected side effects,
517 dual PPAR agonists are likely to be effective as barrier-protective agents. As for side effects,
518 we noted is that balanced PPAR γ / α agonists are rare; while all dual PPAR α / γ agonists that have
519 been discontinued due to side effects happen to be either single (only PPAR γ) or ‘unbalanced’
520 (PPAR γ >> PPAR α agonistic activity), the newer generation formulations that are currently in
521 the clinical trial have a reversed agonistic potency (PPAR α >> PPAR γ agonistic activity) (see
522 **Table 3**). Because macrophage responses require finetuning (discussed below), our studies
523 show how unopposed agonism of either PPAR γ or PPAR α is harmful and can
524 impair/dysregulate the way macrophages respond when microbes breach past the gut barrier.
525 It is possible that many of the side effects of the discontinued thiazolidinediones are due to
526 their inability to achieve that ‘optimal’ spectrum of macrophage function.

527 *Third*, when it comes to macrophage biology, this work sheds some unexpected and
528 previously unforeseen insights into the role of the PPARs in the regulation of macrophage
529 processes. Extensively studied for over ~3 decades, PPARs are known to regulate macrophage
530 activation in health and disease⁶⁴. Targeting PPARs as a host-directed treatment approach to
531 infectious/inflammatory diseases appears to be a sound strategy because they regulate
532 macrophage lipid metabolism, cholesterol efflux, inflammatory responses (ROS and cytokine
533 production), apoptosis, and production of antimicrobial byproducts⁶⁵. We found that
534 unopposed PPAR γ activation suppresses bacterial clearance and blunts the induction of
535 proinflammatory (but not anti-inflammatory, IL10) cytokines and ROS in response to infection
536 both *in vivo* and *in vitro*. In other words, and consistent with prior reports, PPAR γ activation
537 suppressed inflammation at the cost of impairing immunity. Our findings are in keeping with
538 the findings of a systematic review and meta-analysis of 13 long-term randomized controlled
539 trials that involved 17,627 participants (8,163 receiving PPAR γ agonists and 9,464 receiving
540 control drugs)⁶⁶. Long-term (~1–5.5 y) use of PPAR γ agonists increases the risk of pneumonia
541 or lower respiratory tract infection significantly, some of which result in hospitalization,
542 disability, or death⁶⁶. In the case of PPAR α , unopposed activation-induced ROS and
543 proinflammatory cytokines and accelerated bacterial clearance. Inhibitor studies further
544 confirmed that PPAR α was required for these responses (**Fig 5**). These findings are in keeping
545 with others’ showing that PPAR α , but not PPAR γ is required for NADPH-induced ROS
546 formation both in human and murine macrophages⁶⁷. PPAR α agonists induce the expression
547 of NADPH oxidase subunits p47(phox), p67phox, and gp91phox, which are all essential
548 functional components of NADPH complex⁶⁷. Dual and balanced PPAR α / γ agonism enhanced

549 bacterial clearance with only a moderate induction of proinflammatory cytokines or ROS. Such
 550 a response ensures that the macrophage functions within a ‘goldilocks’ zone, mounting
 551 inflammation that is just sufficient for microbial clearance and immunity. In our analysis, the
 552 only other PPAR-related gene within the IBD network, i.e., PGC1a, and its role within the
 553 PPAR α/γ axis suggests that the intricate network of forward feedback loops orchestrated by
 554 PGC1a may be critical for achieving the critical balance between immunity and inflammation,
 555 which is a key outcome of the dual PPAR α/γ agonists.

556 Because previous studies using cell-specific gene depletion have indicated that the
 557 barrier-protective role of PPAR γ may be mediated *via* cells other than the macrophages ⁴⁸,
 558 namely, the T cells ⁶⁸ and the epithelial cells ⁶⁹, it is possible that the dual PPAR α/γ agonists
 559 also act on those cells, promoting bacterial clearance and balancing cellular bioenergetics, ROS
 560 and cytokine production, in manners similar to that we observe in macrophages.

561 Taken together, our study uses an unconventional approach to rationalize and validate
 562 the use of PPAR α/γ dual agonists as first-in-class barrier protective macrophage modulators in
 563 the management of IBD. The approach is powerful because it leverages the precision of
 564 mathematics (*Boolean algebra of logic*) and the fundamental invariant patterns in gene
 565 expression (Boolean Implications). The AI-navigated drug discovery approach defined here
 566 could serve as a blueprint for future studies not just in IBD, but in any other such complex
 567 chronic diseases.

568

569 AUTHOR CONTRIBUTIONS

Role	Authors
Conceptualization; Supervision; Project administration	
<ul style="list-style-type: none"> • Conceptualization (PG and GDK) • Supervision (PG, SD, DS) • Project Administration (PG) 	PG, DS, SD and GDK
Investigation; Methodology; Data curation, Formal Analysis	GDK, VC, MSA, EV, IMS, DT, FU, JRS, SD
<ul style="list-style-type: none"> • Animal studies (GDK, VC, MSA, IMS, FU) • Cell and tissue analysis (qPCR, ROS, bacterial clearance, ELISA)- (GDK, VC, MSA, IMS, DT, FU, SD) • Computational modeling (DS) • Computational analysis (DS) 	
Funding acquisition	DS, SD, PG
Resources	JRS, GL, JY, WJS
Software	DS
Visualization; Writing – original draft; Writing – review & editing	GDK, DS, PG

570 **ACKNOWLEDGMENTS**

571

572 We thank Dharanidhar Dang (UCSD) for comments and critiques during the preparation of the
573 manuscript. This work was supported by National Institutes for Health (NIH) grants R01-
574 AI141630 (to PG), DK107585 (to SD). PG, SD, and DS were also supported by the Leona M.
575 and Harry B. Helmsley Charitable Trust and the NIH (UG3TR003355, UG3TR002968 and
576 R01-AI55696). GDK was supported through The American Association of Immunologists
577 Intersect Fellowship Program for Computational Scientists and Immunologists. J.S.
578 acknowledges support from the Interfaces Training Grant at UCSD (NIH T32EB009380).
579 Authors thank to Lee Swanson, Courtney Tindle, Stella-Rita Ibeawuchi, Julian Tam and
580 Madhubanti Mullick for their comments, feedback and technical support.
581 This manuscript includes data generated at the UC San Diego Institute of Genomic Medicine
582 (IGC) using an Illumina NovaSeq 6000 that was purchased with funding from a National
583 Institutes of Health SIG grant (#S10 OD026929). Additionally, a P30 grant (NIH/NIDDK,
584 P30DK120515) subsidized the RNA Seq and histology work showcased here.

585

586 **CODE AVAILABILITY**

587 The codes are publicly available at the following links: <https://github.com/sahoo00/BoNE>;
588 <https://github.com/sahoo00/Hegemon>

589 **REFERENCES**

590

- 591 1 Richard, M. L. & Sokol, H. The gut mycobiota: insights into analysis, environmental
592 interactions and role in gastrointestinal diseases. *Nat Rev Gastroenterol Hepatol* **16**,
593 331-345, doi:10.1038/s41575-019-0121-2 (2019).
- 594 2 Schirmer, M., Garner, A., Vlamakis, H. & Xavier, R. J. Microbial genes and pathways
595 in inflammatory bowel disease. *Nat Rev Microbiol* **17**, 497-511, doi:10.1038/s41579-
596 019-0213-6 (2019).
- 597 3 Lavelle, A. & Sokol, H. Gut microbiota-derived metabolites as key actors in
598 inflammatory bowel disease. *Nat Rev Gastroenterol Hepatol*, doi:10.1038/s41575-019-
599 0258-z (2020).
- 600 4 Furey, T. S., Sethupathy, P. & Sheikh, S. Z. Redefining the IBDs using genome-scale
601 molecular phenotyping. *Nat Rev Gastroenterol Hepatol* **16**, 296-311,
602 doi:10.1038/s41575-019-0118-x (2019).
- 603 5 Olivera, P., Danese, S., Jay, N., Natoli, G. & Peyrin-Biroulet, L. Big data in IBD: a
604 look into the future. *Nat Rev Gastroenterol Hepatol* **16**, 312-321, doi:10.1038/s41575-
605 019-0102-5 (2019).
- 606 6 Moschen, A. R., Tilg, H. & Raine, T. IL-12, IL-23 and IL-17 in IBD: immunobiology
607 and therapeutic targeting. *Nat Rev Gastroenterol Hepatol* **16**, 185-196,
608 doi:10.1038/s41575-018-0084-8 (2019).
- 609 7 Ahluwalia, J. P. Immunotherapy in inflammatory bowel disease. *Med Clin North Am*
610 **96**, 525-544, x, doi:10.1016/j.mcna.2012.04.009 (2012).

- 611 8 Na, Y. R., Stakenborg, M., Seok, S. H. & Matteoli, G. Macrophages in intestinal
612 inflammation and resolution: a potential therapeutic target in IBD. *Nat Rev*
613 *Gastroenterol Hepatol* **16**, 531-543, doi:10.1038/s41575-019-0172-4 (2019).
- 614 9 Debashis, S. *et al.* AI-guided Discovery of a Barrier-Protective Therapy in
615 Inflammatory Bowel Disease. *Nat Commun* (under review 2020).
- 616 10 Kim, S. H. *et al.* MD001, a Novel Peroxisome Proliferator-activated Receptor α/γ
617 Agonist, Improves Glucose and Lipid Metabolism. *Sci Rep* **9**, 1656,
618 doi:10.1038/s41598-018-38281-0 (2019).
- 619 11 Annese, V., Rogai, F., Settesoldi, A. & Bagnoli, S. PPAR γ in Inflammatory
620 Bowel Disease. *PPAR Res* **2012**, 620839, doi:10.1155/2012/620839 (2012).
- 621 12 Auwerx, J. Nuclear receptors. I. PPAR γ in the gastrointestinal tract: gain or pain?
622 *Am J Physiol Gastrointest Liver Physiol* **282**, G581-585, doi:10.1152/ajpgi.00508.2001
623 (2002).
- 624 13 Dubuquoy, L. *et al.* PPAR γ as a new therapeutic target in inflammatory bowel
625 diseases. *Gut* **55**, 1341-1349, doi:10.1136/gut.2006.093484 (2006).
- 626 14 Ramakers, J. D. *et al.* The PPAR γ agonist rosiglitazone impairs colonic
627 inflammation in mice with experimental colitis. *J Clin Immunol* **27**, 275-283,
628 doi:10.1007/s10875-007-9074-2 (2007).
- 629 15 Vetuschi, A., Pompili, S., Gaudio, E., Latella, G. & Sferra, R. PPAR- γ with its
630 anti-inflammatory and anti-fibrotic action could be an effective therapeutic target in
631 IBD. *Eur Rev Med Pharmacol Sci* **22**, 8839-8848, doi:10.26355/eurrev_201812_16652
632 (2018).
- 633 16 Xia, H. *et al.* Protectin DX increases survival in a mouse model of sepsis by
634 ameliorating inflammation and modulating macrophage phenotype. *Sci Rep* **7**, 99,
635 doi:10.1038/s41598-017-00103-0 (2017).
- 636 17 Nagy, L., Szanto, A., Szatmari, I. & Széles, L. Nuclear hormone receptors enable
637 macrophages and dendritic cells to sense their lipid environment and shape their
638 immune response. *Physiol Rev* **92**, 739-789, doi:10.1152/physrev.00004.2011 (2012).
- 639 18 Xu, Z. *et al.* PPAR- γ agonist ameliorates liver pathology accompanied by increasing
640 regulatory B and T cells in high-fat-diet mice. *Obesity (Silver Spring)* **25**, 581-590,
641 doi:10.1002/oby.21769 (2017).
- 642 19 Klotz, L. *et al.* The nuclear receptor PPAR γ selectively inhibits Th17
643 differentiation in a T cell-intrinsic fashion and suppresses CNS autoimmunity. *J Exp*
644 *Med* **206**, 2079-2089, doi:10.1084/jem.20082771 (2009).
- 645 20 Lewis, J. D. *et al.* An open-label trial of the PPAR- γ ligand rosiglitazone for
646 active ulcerative colitis. *Am J Gastroenterol* **96**, 3323-3328, doi:10.1111/j.1572-
647 0241.2001.05333.x (2001).
- 648 21 Huang, Y. *et al.* Pioglitazone Attenuates Experimental Colitis-Associated Hyperalgesia
649 through Improving the Intestinal Barrier Dysfunction. *Inflammation*,
650 doi:10.1007/s10753-019-01138-3 (2020).
- 651 22 Liang, H. L. & Ouyang, Q. A clinical trial of combined use of rosiglitazone and 5-
652 aminosalicylate for ulcerative colitis. *World J Gastroenterol* **14**, 114-119,
653 doi:10.3748/wjg.14.114 (2008).
- 654 23 Ogawa, S., Takeuchi, K. & Ito, S. Plasma BNP levels in the treatment of type 2 diabetes
655 with pioglitazone. *J Clin Endocrinol Metab* **88**, 3993-3996, doi:10.1210/jc.2002-
656 021765 (2003).
- 657 24 Liao, H. W. *et al.* Pioglitazone and cardiovascular outcomes in patients with insulin
658 resistance, pre-diabetes and type 2 diabetes: a systematic review and meta-analysis.
659 *BMJ Open* **7**, e013927, doi:10.1136/bmjopen-2016-013927 (2017).

- 660 25 Cheng, H. S. *et al.* Exploration and Development of PPAR Modulators in Health and
661 Disease: An Update of Clinical Evidence. *Int J Mol Sci* **20**, doi:10.3390/ijms20205055
662 (2019).
- 663 26 Decara, J. *et al.* Peroxisome Proliferator-Activated Receptors: Experimental Targeting
664 for the Treatment of Inflammatory Bowel Diseases. *Front Pharmacol* **11**, 730,
665 doi:10.3389/fphar.2020.00730 (2020).
- 666 27 Dou, X., Xiao, J., Jin, Z. & Zheng, P. Peroxisome proliferator-activated receptor- γ is
667 downregulated in ulcerative colitis and is involved in experimental colitis-associated
668 neoplasia. *Oncol Lett* **10**, 1259-1266, doi:10.3892/ol.2015.3397 (2015).
- 669 28 Dubuquoy, L. *et al.* Impaired expression of peroxisome proliferator-activated receptor
670 gamma in ulcerative colitis. *Gastroenterology* **124**, 1265-1276, doi:10.1016/s0016-
671 5085(03)00271-3 (2003).
- 672 29 Poliska, S. *et al.* Association of peroxisome proliferator-activated receptor gamma
673 polymorphisms with inflammatory bowel disease in a Hungarian cohort. *Inflamm
674 Bowel Dis* **18**, 472-479, doi:10.1002/ibd.21798 (2012).
- 675 30 Hugot, J. P. PPAR and Crohn's disease: another piece of the puzzle? *Gastroenterology*
676 **128**, 500-503, doi:10.1053/j.gastro.2004.12.041 (2005).
- 677 31 Zhang, Z. F., Yang, N., Zhao, G., Zhu, L. & Wang, L. X. Association between the
678 Pro12Ala polymorphism of peroxisome proliferator-activated receptor gamma 2 and
679 inflammatory bowel disease: a meta-analysis. *PLoS One* **7**, e30551,
680 doi:10.1371/journal.pone.0030551 (2012).
- 681 32 Takada, I. & Makishima, M. Peroxisome proliferator-activated receptor agonists and
682 antagonists: a patent review (2014-present). *Expert Opin Ther Pat* **30**, 1-13,
683 doi:10.1080/13543776.2020.1703952 (2020).
- 684 33 Mirza, A. Z., Althagafi, II & Shamshad, H. Role of PPAR receptor in different diseases
685 and their ligands: Physiological importance and clinical implications. *Eur J Med Chem*
686 **166**, 502-513, doi:10.1016/j.ejmech.2019.01.067 (2019).
- 687 34 Jain, M. R. *et al.* Saroglitazar, a novel PPAR α/γ agonist with predominant PPAR α
688 activity, shows lipid-lowering and insulin-sensitizing effects in preclinical models.
689 *Pharmacol Res Perspect* **3**, e00136, doi:10.1002/prp2.136 (2015).
- 690 35 Kim, M. K. *et al.* PAR-5359, a well-balanced PPAR α/γ dual agonist, exhibits
691 equivalent antidiabetic and hypolipidemic activities in vitro and in vivo. *Eur J
692 Pharmacol* **595**, 119-125, doi:10.1016/j.ejphar.2008.07.066 (2008).
- 693 36 Kim, D. K. *et al.* Liquid chromatography-tandem mass spectrometry of a new
694 PPAR α/γ dual agonist PAR-5359 in rat plasma. *Arch Pharm Res* **32**, 1743-
695 1748, doi:10.1007/s12272-009-2212-z (2009).
- 696 37 Brown, P. J. *et al.* Identification of a subtype selective human PPAR α agonist
697 through parallel-array synthesis. *Bioorg Med Chem Lett* **11**, 1225-1227,
698 doi:10.1016/s0960-894x(01)00188-3 (2001).
- 699 38 Information, N. C. f. B. *PubChem Compound Summary for CID 4829, Pioglitazone*,
700 (2020).
- 701 39 Koroleva, E. P. *et al.* Citrobacter rodentium-induced colitis: A robust model to study
702 mucosal immune responses in the gut. *J Immunol Methods* **421**, 61-72,
703 doi:10.1016/j.jim.2015.02.003 (2015).
- 704 40 Bosman, E. S., Chan, J. M., Bhullar, K. & Vallance, B. A. Investigation of Host and
705 Pathogen Contributions to Infectious Colitis Using the Citrobacter rodentium Mouse
706 Model of Infection. *Methods Mol Biol* **1422**, 225-241, doi:10.1007/978-1-4939-3603-
707 8_21 (2016).
- 708 41 Bhinder, G. *et al.* The Citrobacter rodentium mouse model: studying pathogen and host
709 contributions to infectious colitis. *J Vis Exp*, e50222, doi:10.3791/50222 (2013).

- 710 42 Krause, P. *et al.* IL-10-producing intestinal macrophages prevent excessive
711 antibacterial innate immunity by limiting IL-23 synthesis. *Nat Commun* **6**, 7055,
712 doi:10.1038/ncomms8055 (2015).
- 713 43 Jiminez, J. A., Uwiera, T. C., Douglas Inglis, G. & Uwiera, R. R. Animal models to
714 study acute and chronic intestinal inflammation in mammals. *Gut Pathog* **7**, 29,
715 doi:10.1186/s13099-015-0076-y (2015).
- 716 44 Kozaiwa, K. *et al.* Identification of a quantitative trait locus for ileitis in a spontaneous
717 mouse model of Crohn's disease: SAMP1/YitFc. *Gastroenterology* **125**, 477-490,
718 doi:10.1016/s0016-5085(03)00876-x (2003).
- 719 45 Qi, Y. *et al.* PPARalpha-dependent exacerbation of experimental colitis by the
720 hypolipidemic drug fenofibrate. *Am J Physiol Gastrointest Liver Physiol* **307**, G564-
721 573, doi:10.1152/ajpgi.00153.2014 (2014).
- 722 46 Gu, X. *et al.* GC-MS metabolomics on PPARalpha-dependent exacerbation of colitis.
723 *Mol Biosyst* **11**, 1329-1337, doi:10.1039/c5mb00048c (2015).
- 724 47 Mohapatra, S. K. *et al.* Immunoregulatory actions of epithelial cell PPAR gamma at the
725 colonic mucosa of mice with experimental inflammatory bowel disease. *PLoS One* **5**,
726 e10215, doi:10.1371/journal.pone.0010215 (2010).
- 727 48 Hontecillas, R. *et al.* Immunoregulatory mechanisms of macrophage PPAR- γ in mice
728 with experimental inflammatory bowel disease. *Mucosal Immunol* **4**, 304-313,
729 doi:10.1038/mi.2010.75 (2011).
- 730 49 Guri, A. J., Mohapatra, S. K., Horne, W. T., 2nd, Hontecillas, R. & Bassaganya-Riera,
731 J. The role of T cell PPAR gamma in mice with experimental inflammatory bowel
732 disease. *BMC Gastroenterol* **10**, 60, doi:10.1186/1471-230x-10-60 (2010).
- 733 50 Boudeau, J., Glasser, A. L., Masseret, E., Joly, B. & Darfeuille-Michaud, A. Invasive
734 ability of an Escherichia coli strain isolated from the ileal mucosa of a patient with
735 Crohn's disease. *Infect Immun* **67**, 4499-4509 (1999).
- 736 51 Pavlou, S., Wang, L., Xu, H. & Chen, M. Higher phagocytic activity of thioglycollate-
737 elicited peritoneal macrophages is related to metabolic status of the cells. *J Inflamm*
738 *(Lond)* **14**, 4, doi:10.1186/s12950-017-0151-x (2017).
- 739 52 Layoun, A., Samba, M. & Santos, M. M. Isolation of murine peritoneal macrophages
740 to carry out gene expression analysis upon Toll-like receptors stimulation. *J Vis Exp*,
741 e52749, doi:10.3791/52749 (2015).
- 742 53 Tan, H. Y. *et al.* The Reactive Oxygen Species in Macrophage Polarization: Reflecting
743 Its Dual Role in Progression and Treatment of Human Diseases. *Oxid Med Cell Longev*
744 **2016**, 2795090, doi:10.1155/2016/2795090 (2016).
- 745 54 Tan, H.-Y. *et al.* The Reactive Oxygen Species in Macrophage Polarization: Reflecting
746 Its Dual Role in Progression and Treatment of Human Diseases. *Oxidative Medicine*
747 *and Cellular Longevity* **2016**, 2795090, doi:10.1155/2016/2795090 (2016).
- 748 55 Segal, A. W. Studies on patients establish Crohn's disease as a manifestation of
749 impaired innate immunity. *J Intern Med* **286**, 373-388, doi:10.1111/joim.12945 (2019).
- 750 56 Baillie, J. K. *et al.* Analysis of the human monocyte-derived macrophage transcriptome
751 and response to lipopolysaccharide provides new insights into genetic aetiology of
752 inflammatory bowel disease. *PLoS Genet* **13**, e1006641,
753 doi:10.1371/journal.pgen.1006641 (2017).
- 754 57 Quezada, S. M., McLean, L. P. & Cross, R. K. Adverse events in IBD therapy: the 2018
755 update. *Expert Rev Gastroenterol Hepatol* **12**, 1183-1191,
756 doi:10.1080/17474124.2018.1545574 (2018).
- 757 58 Harris, M. S., Wichary, J., Zadnik, M. & Reinisch, W. Competition for Clinical Trials
758 in Inflammatory Bowel Diseases. *Gastroenterology* **157**, 1457-1461.e1452,
759 doi:10.1053/j.gastro.2019.08.020 (2019).

- 760 59 Zhou, X. *et al.* PPARalpha-UGT axis activation represses intestinal FXR-FGF15
761 feedback signalling and exacerbates experimental colitis. *Nat Commun* **5**, 4573,
762 doi:10.1038/ncomms5573 (2014).
- 763 60 Manoharan, I. *et al.* Homeostatic PPARalpha Signaling Limits Inflammatory
764 Responses to Commensal Microbiota in the Intestine. *J Immunol* **196**, 4739-4749,
765 doi:10.4049/jimmunol.1501489 (2016).
- 766 61 Azuma, Y. T. *et al.* PPARalpha contributes to colonic protection in mice with DSS-
767 induced colitis. *Int Immunopharmacol* **10**, 1261-1267,
768 doi:10.1016/j.intimp.2010.07.007 (2010).
- 769 62 Lewis, J. D. *et al.* Rosiglitazone for active ulcerative colitis: a randomized placebo-
770 controlled trial. *Gastroenterology* **134**, 688-695, doi:10.1053/j.gastro.2007.12.012
771 (2008).
- 772 63 Pedersen, G. & Brynskov, J. Topical rosiglitazone treatment improves ulcerative colitis
773 by restoring peroxisome proliferator-activated receptor-gamma activity. *Am J*
774 *Gastroenterol* **105**, 1595-1603, doi:10.1038/ajg.2009.749 (2010).
- 775 64 Chawla, A. Control of macrophage activation and function by PPARs. *Circ Res* **106**,
776 1559-1569, doi:10.1161/circresaha.110.216523 (2010).
- 777 65 Leopold Wager, C. M., Arnett, E. & Schlesinger, L. S. Macrophage nuclear receptors:
778 Emerging key players in infectious diseases. *PLoS Pathog* **15**, e1007585,
779 doi:10.1371/journal.ppat.1007585 (2019).
- 780 66 Singh, S., Loke, Y. K. & Furberg, C. D. Long-term use of thiazolidinediones and the
781 associated risk of pneumonia or lower respiratory tract infection: systematic review and
782 meta-analysis. *Thorax* **66**, 383-388, doi:10.1136/thx.2010.152777 (2011).
- 783 67 Teissier, E. *et al.* Peroxisome proliferator-activated receptor alpha induces NADPH
784 oxidase activity in macrophages, leading to the generation of LDL with PPAR-alpha
785 activation properties. *Circ Res* **95**, 1174-1182,
786 doi:10.1161/01.Res.0000150594.95988.45 (2004).
- 787 68 Guri, A. J., Evans, N. P., Hontecillas, R. & Bassaganya-Riera, J. T cell PPARgamma
788 is required for the anti-inflammatory efficacy of abscisic acid against experimental
789 IBD. *J Nutr Biochem* **22**, 812-819, doi:10.1016/j.jnutbio.2010.06.011 (2011).
- 790 69 Hontecillas, R. & Bassaganya-Riera, J. Expression of PPAR gamma in intestinal
791 epithelial cells is dispensable for the prevention of colitis by dietary abscisic acid. *Espen*
792 *j* **7**, e189-e195, doi:10.1016/j.clnme.2012.07.002 (2012).
- 793
- 794

FIGURES AND LEGENDS

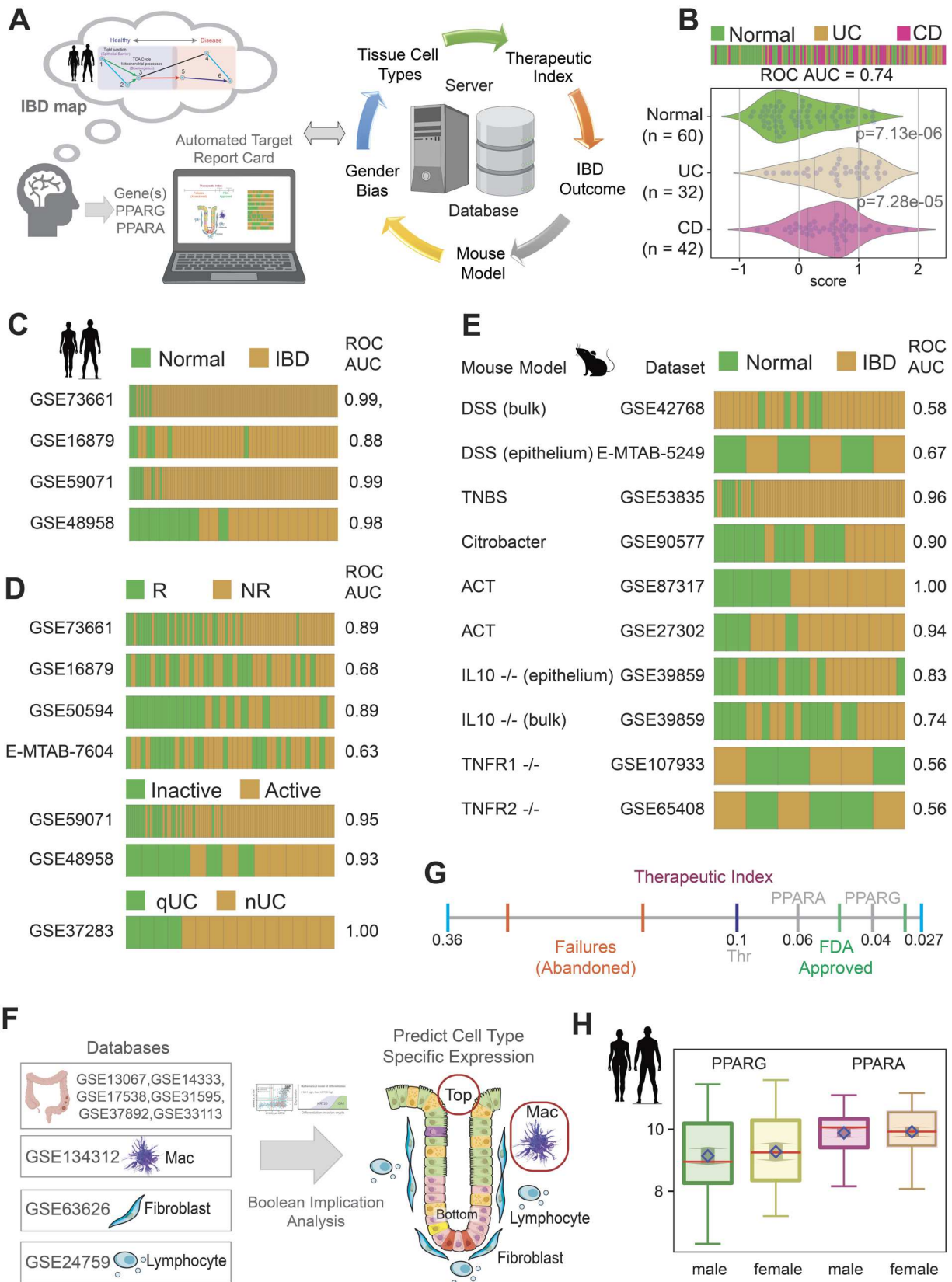


Figure 1: Network-rationalized target identification and study design. (A) Schematic displays the overall computationally guided study design. An interactive web-based platform allows the querying of paths of gene clusters in the IBD map [9; see **Supplementary Fig. 1**] to pick high-value targets with a few mouse clicks and

801 generate a comprehensive automated target ‘report card’. The components of a ‘target report card’ is shown
802 (*right*): predicted ‘therapeutic index’ (likelihood of Phase III success), IBD outcome (prognostic potential in UC
803 and/or CD), network-prioritized mouse model, estimation of gender bias and predicted tissue cell type of action.
804 **(B-H)** Components of a target report card for PPARA and PPARG are displayed. Bar plot (B; top) displays the
805 rank ordering of normal vs ulcerative colitis (UC) /Crohn’s Disease (CD) patient samples using the average gene
806 expression patterns of the two genes: PPARG/PPARA. ROC-AUC statistics were measured for determining the
807 classification strength of normal vs IBD. Bar plots (B; top) and violin plots (B; bottom) display the differences in
808 the average expression of the two genes in normal, UC and CD samples in the test cohort used to build the IBD-
809 map. Bar plots in panel C-D show the rank ordering of either normal vs IBD samples (C) or responder vs non-
810 responder (R vs. NR; D), or active vs inactive disease, or neoplastic progression in quiescent UC (qUC vs. nUC;
811 D) across numerous cohorts based on gene expression patterns of PPARG and PPARA, from high to low, left to
812 right. Classification strength within each cohort is measured using ROC-AUC analyses. Bar plots in panel E show
813 the rank ordering of either normal vs IBD samples across numerous published murine models of IBD based on
814 gene expression patterns of PPARG and PPARA as in D. ACT = adoptive T cell transfer. Classification strength
815 within each cohort is measured using ROC-AUC analyses. Bulk = whole distal colon; epithelium = sorted
816 epithelial cells. Schematic in F summarizes the computational prediction of the cell type of action for potential
817 PPARA/G targeted therapy, as determined using Boolean implication analysis. GSEID# of multiple publicly
818 available databases of the different cell types and colorectal datasets used to make sure predictions are cited. Red
819 boxes/circles denote that PPARA/G-targeted therapeutics are predicted to work on monocytes/macrophages and
820 crypt-top enterocytes. Computationally generated therapeutic index (see *Methods*) is represented as a line graph
821 in G. The annotated numbers represent Boolean implication statistics. PPARA and PPARG align with FDA
822 approved targets on the right of threshold (0.1). Two FDA approved targets (green; ITGB1, 0.046; JAK2, 0.032),
823 two abandoned targets (red; SMAD7, 0.33; IL11, 0.16), PPARA (grey, 0.064), PPARG (grey, 0.04), and the
824 threshold (black, 0.1) are shown in the scale. Box plot in panel H shows that the level of PPARA/G expression is
825 similar in the colons of both genders in health and in IBD, and hence, PPARA/G-targeted therapeutics are predicted
826 to have little/no gender predilection.

827
828
829
830
831
832
833
834
835
836
837
838
839
840
841
842
843
844
845
846
847
848
849
850
851
852
853
854

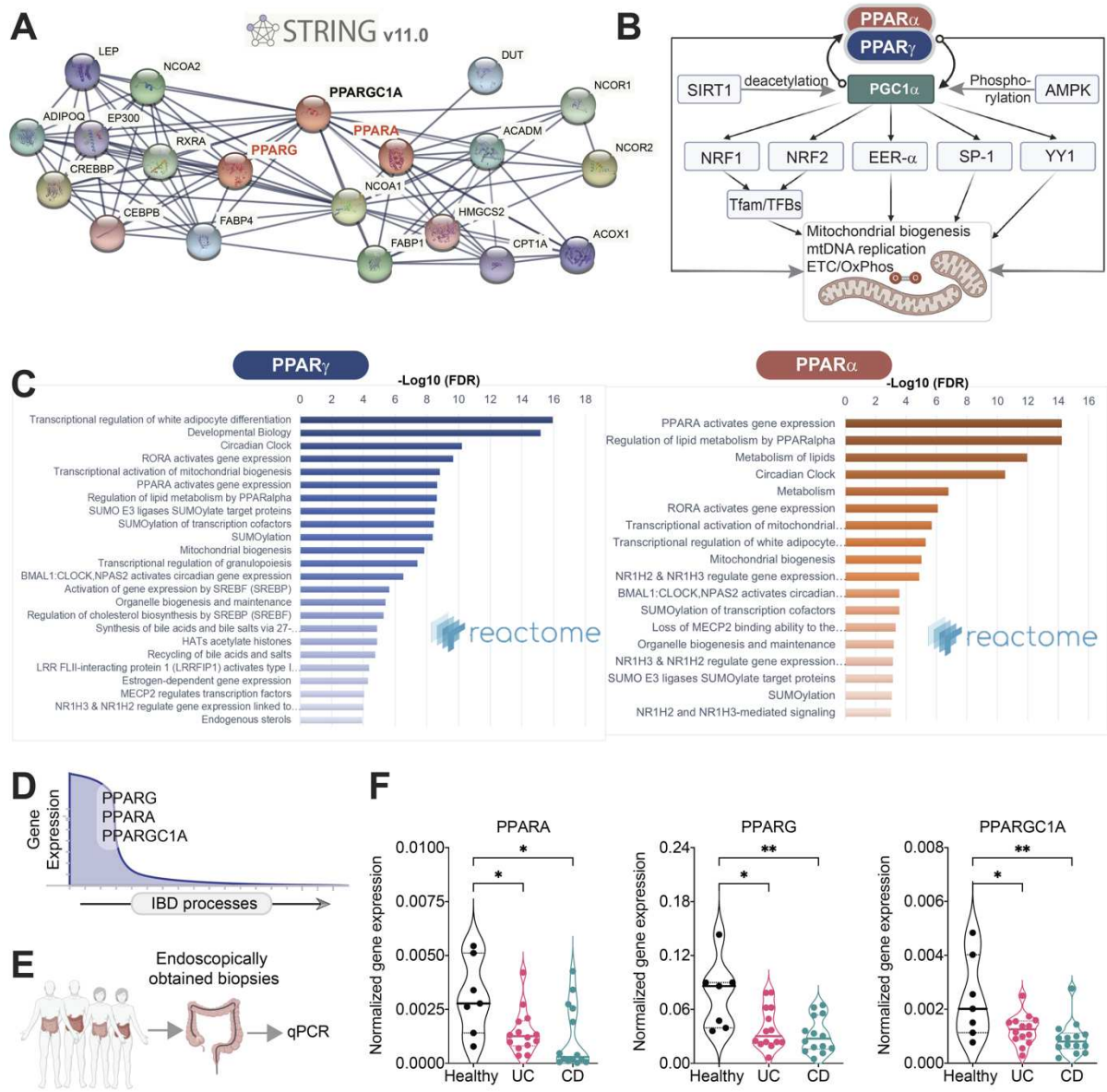
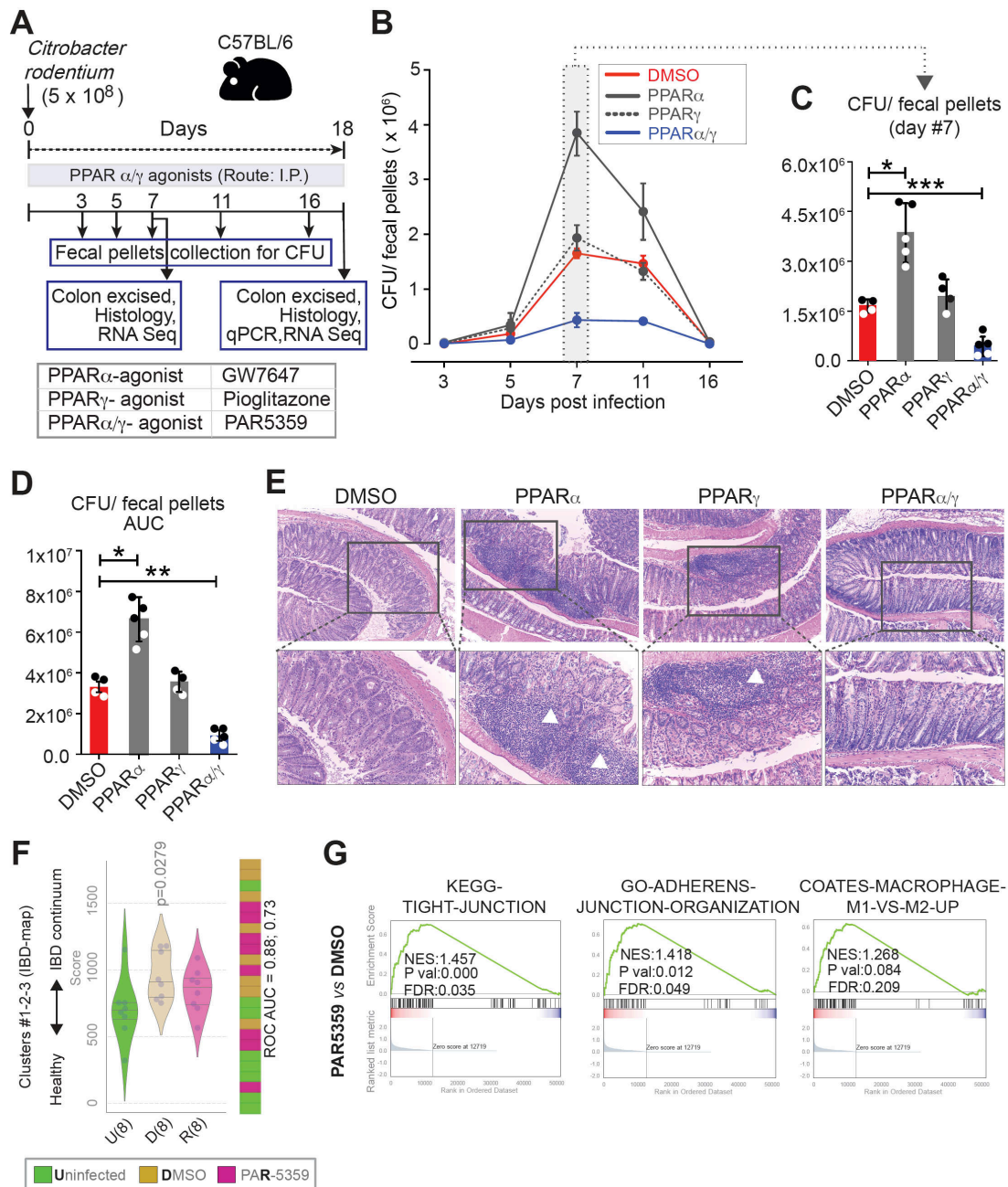


Figure 2: Rationalization of PPAR α and PPAR γ as targets in IBD.

(A) A protein-protein interaction network (i.e., interactomes) for PPAR α and PPAR γ , generated using STRING v.11 (<https://string-db.org>). (B) Schematic summarizing the roles of PPAR α , PPAR γ and PGC1 α on mitochondria biogenesis and function (based on). PGC1- α emerges as a critical hub for forward feedback loops. (C) Reactome pathway analyses (www.reactome.org) on PPAR- α and PPAR- γ interactomes in A show convergence on metabolism, mitochondria bioenergetics and the circadian clock. (D) Graphical visualization of the predicted changes in the expression of PPARA (PPAR- α), PPARG (PPAR- γ) and PPARGC1A (PGC1- α) genes during the progression of IBD processes (indicated with an arrow). (E) Schematic showing validation workflow; the expression of PPARA, PPARG and PPARGC1A transcript levels were assessed in the ileum/colon biopsies of IBD patients (UC=14 and CD= 14) or healthy controls (n=7). (F) Violin plots display the qPCR results in E. Results are displayed as mean \pm SEM. Significance was tested using one-way ANOVA followed by Tukey's test for multiple comparisons. Significance: *, $p < 0.05$; **, $p < 0.01$.

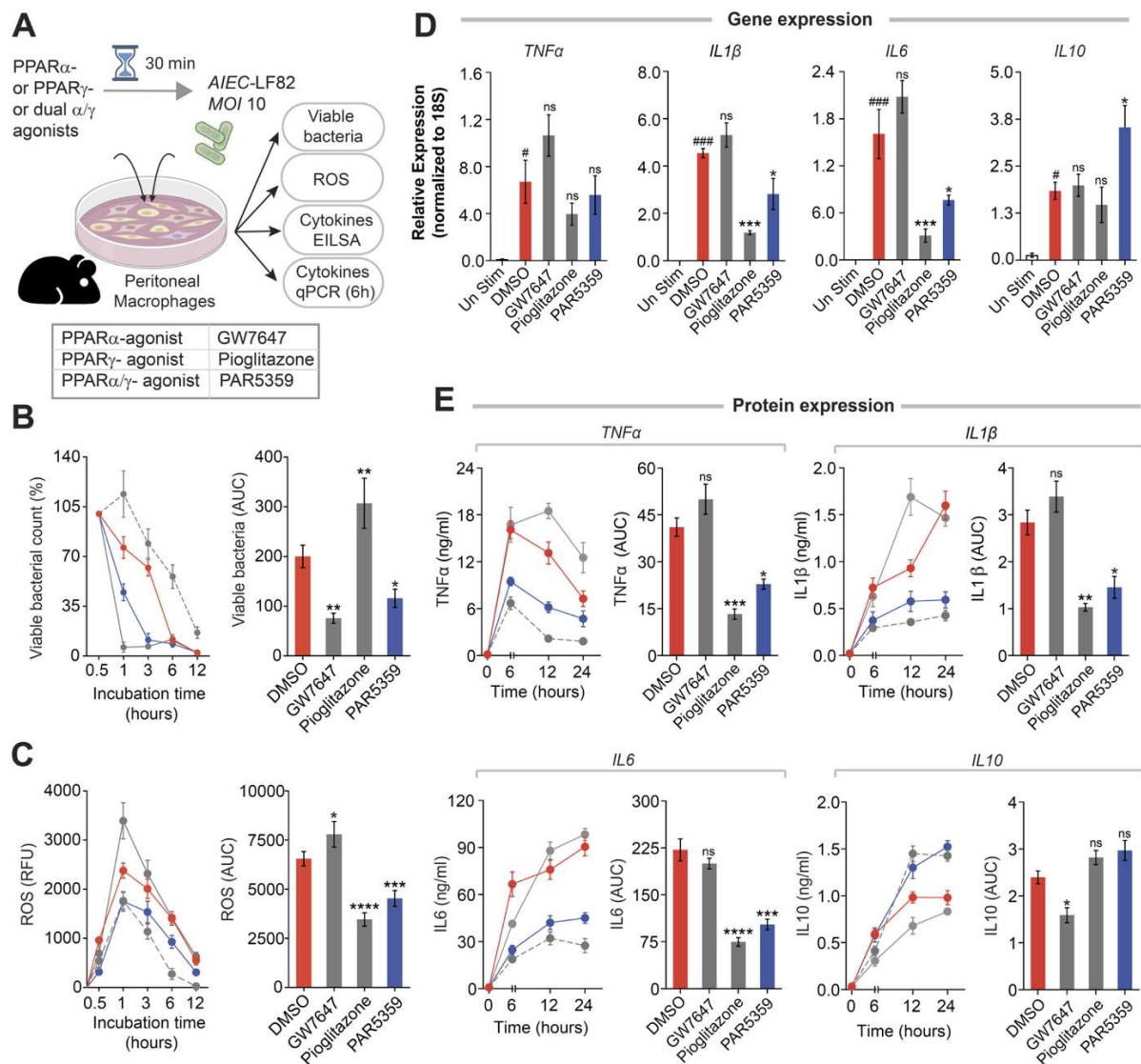
855
856
857
858
859
860
861
862
863
864
865
866
867
868
869
870
871



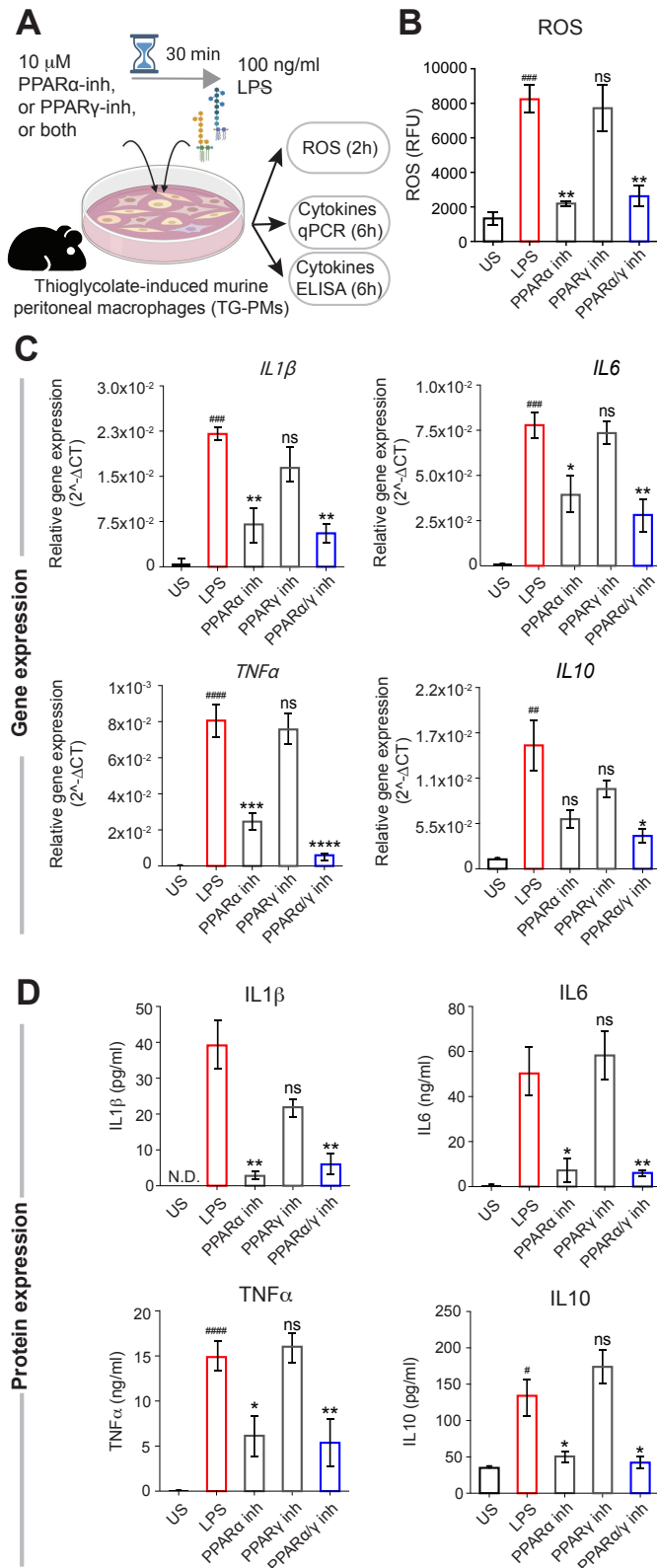
872
873
874
875
876
877
878
879
880
881
882
883
884
885
886
887
888
889

Figure 3: PPAR_{α/γ} dual agonists ameliorate *Citrobacter rodentium*-induced infectious colitis in mice.

(A) Schematic summarizing the workflow for testing PPAR-targeted therapeutics in *C. rodentium*-induced colitis. Mice were gavaged with *C. rodentium* on day 0 and subsequently treated daily with PPAR agonists. Fecal pellets were collected to test viable bacterial burden, as determined by dilution plating and colony counting. Colons were excised on day 7 and 18 and analyzed using the indicated readouts. (B-D) Line graphs in B display time series of the burden of viable bacteria in feces. Scatter plots with bar graphs in C compare the peak burden of viable bacteria in feces on day 7. Scatter plots with bar graphs in D display the area under the curve (AUC) for the line graph in B. (E) Images display representative fields from H&E-stained colon tissues. Mag = 100x (top) and 200x (bottom). White arrowheads point to immune cell infiltrates. Statistics: All results are displayed as mean ± SEM. Significance was tested using two-way/one-way ANOVA followed by Tukey's test for multiple comparisons. Significance: *, p < 0.05; **, p < 0.01, ***, p < 0.001. (F) Violin plots (left) display the deviation of expression of genes in Clusters #1-2-3 in the IBD network, as determined by RNA Seq on murine colons. Bar plot (right) displays the rank ordering of the samples. (G) Pre-ranked GSEA based on pairwise differential expression analyses (DMSO vs PAR5359 groups) are displayed as enrichment plots for epithelial tight (left) and adherens (middle) junction signatures and balanced macrophage processes (right). See also Supplementary Fig. 7 for the Day #7 results in the *C. rodentium*-induced colitis model, Supplementary Fig. 8 for extended GSEA analyses, and Supplementary Fig. 9 for the effect of PAR5359 on DSS-induced colitis in mice.



890
 891 **Figure 4: PPAR α and PPAR α/γ -dual agonists enhance, whereas PPAR γ agonist delay bacterial (*AIEC-LF82*) clearance.**
 892 (A) Schematic displays the experimental design and workflow. Thioglycolate-induced murine
 893 peritoneal macrophages (TG-PM) pretreated with PPAR agonists (see box, below; 20 nM GW7647, 10 μ M
 894 Pioglitazone and 1 μ M PAR5359) were infected with *AIEC-LF82* (MOI 10) and subsequently analyzed for the
 895 bacterial count (Gentamycin protection assay), generation of cellular ROS, secretion of inflammatory cytokines
 896 (in supernatant media by ELISA) and the induction of cytokines (gene transcript analysis by qPCR). (B) Line
 897 graphs (left) display percent viable bacterial counts at indicated times after infection. Bar graphs (right) display
 898 the AUC. (C) Line graphs (left) and bar graphs (right) display the extent of ROS generation over time. (D) Bar
 899 graphs display the relative expression of transcripts of multiple cytokines (IL1 β , IL6, TNF α and IL10). (E) Line
 900 graphs (left) and bar graphs (right) showing the levels of secreted cytokines in the media. Statistics: All results
 901 are from at least three independent experiments and results displayed as means \pm SEM. Significance was tested
 902 using two-way/one-way ANOVA followed by Tukey's test for multiple comparisons. Significance: '#'
 903 significance over uninfected TG-PMs and '*' shows significance over *AIEC-LF82* infected cells. ns, non-
 904 significant, *, $p < 0.05$; **, $p < 0.01$, ***, $p < 0.001$, ****, $p < 0.0001$. See **Supplementary Fig. 10** for similar
 905 bacterial clearance assays performed using *Salmonella enteritica*.
 906
 907
 908
 909
 910
 911
 912
 913



914
915
916
917
918
919
920
921
922

Figure 5: PPAR α but not PPAR γ is required for induction of cellular ROS and proinflammatory cytokines. (A) Schematic of experimental design. TG-PMs were pre-incubated with 10 μ M PPAR α or PPAR γ inhibitors, either alone or in combination for 30 min prior to stimulation with 100 ng/ml LPS. Cells were analyzed at 2 and 6 h to estimate cellular ROS and cytokine induction, respectively. (B-D) Bar graphs display the levels of cellular ROS (B), relative levels of mRNA (C) and protein (D) expression of cytokines (IL1 β , IL6, TNF α and IL10). Statistics: Results are from three independent experiments and displayed as mean \pm SEM. One-way ANOVA followed by Tukey's test for multiple comparisons was performed to test significance. Significance: ns: non-significant, *, $p < 0.05$; **, $p < 0.01$; ***, $p < 0.001$ and ****, $p < 0.0001$.

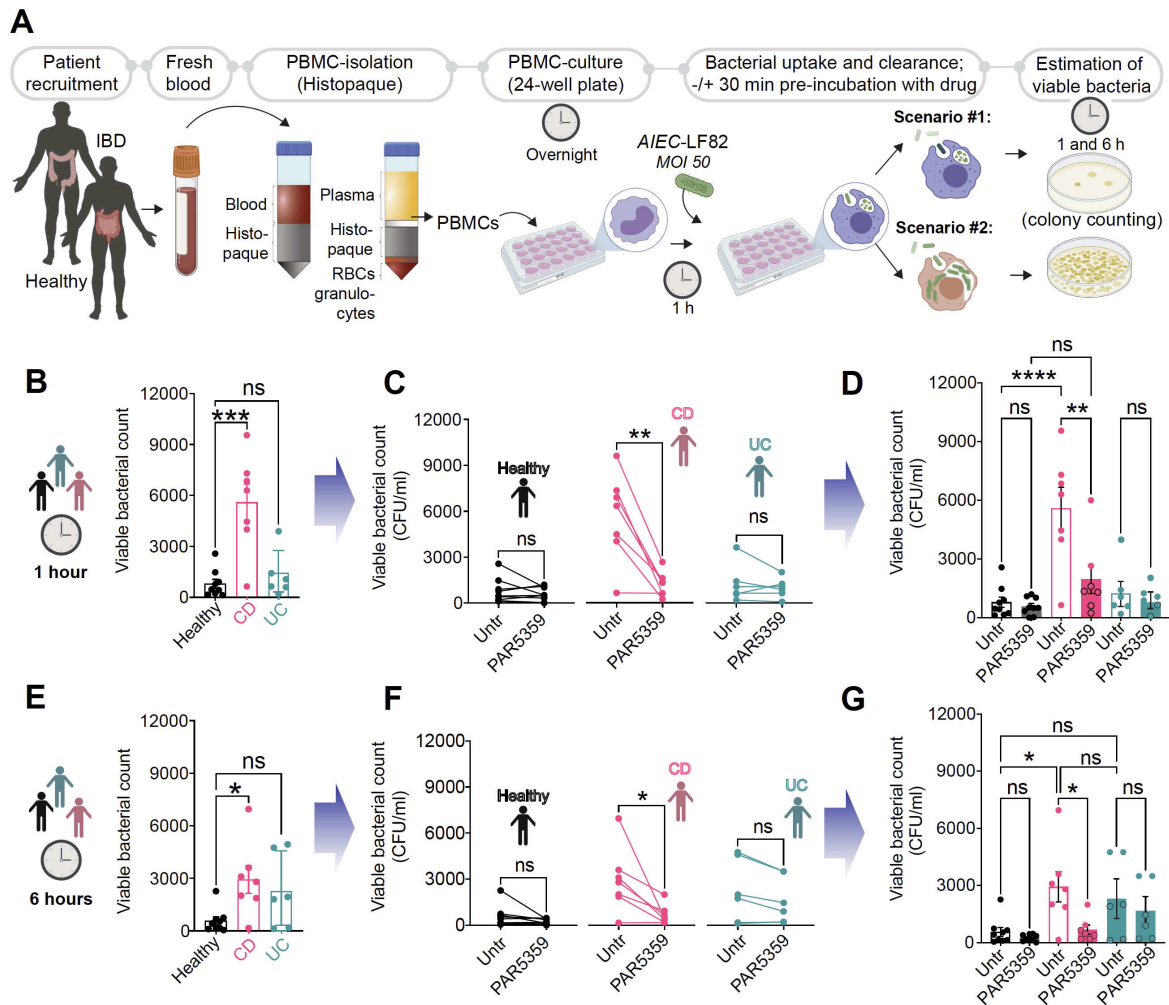
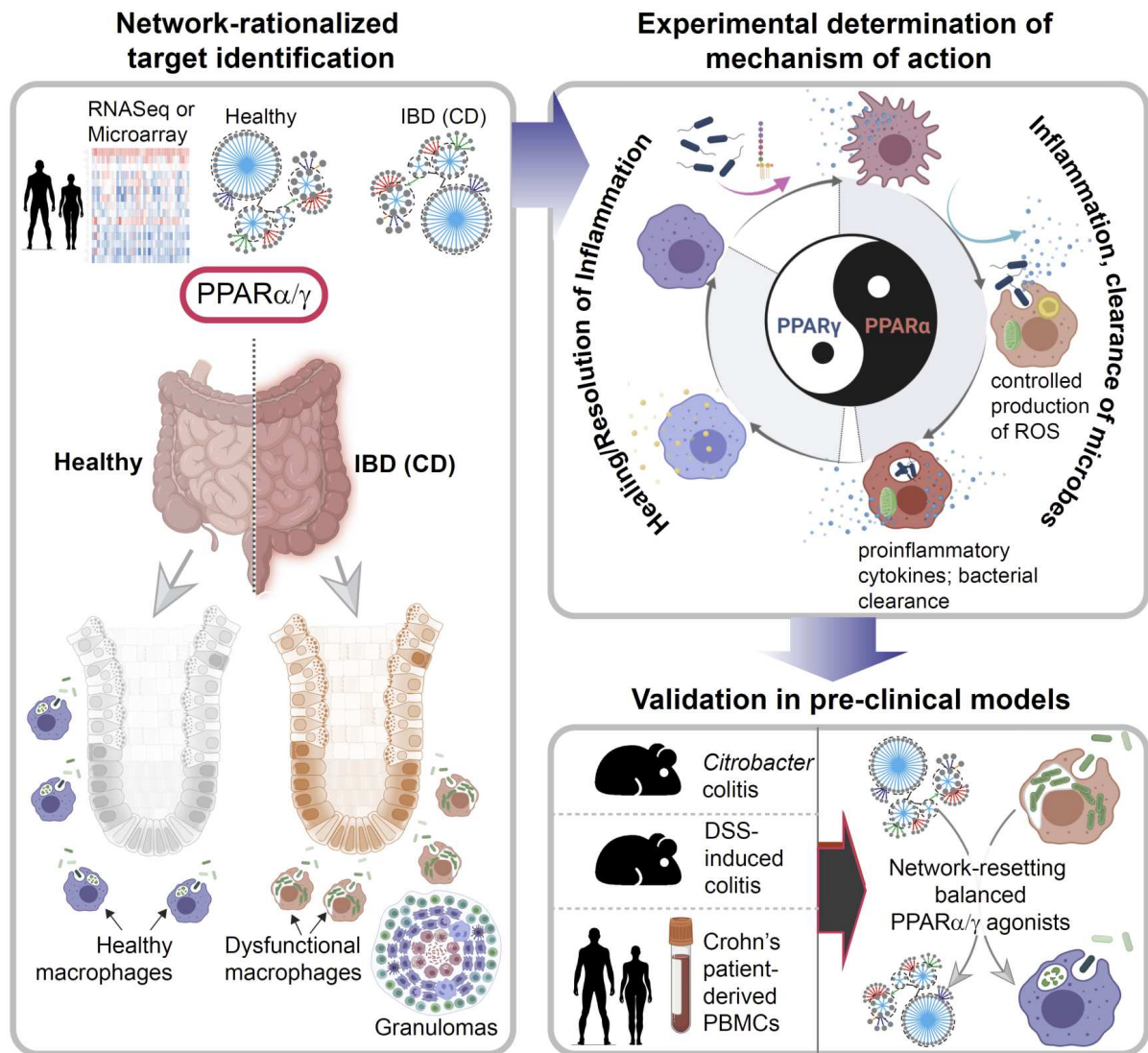


Figure 6: PPAR α/γ dual agonist, PAR5359, promotes the clearance of *AIEC-LF82* from CD patient-derived PBMCs. (A) Schematic displays the overall experimental design using human subjects (see Table 5 for patient demographics). Peripheral blood collected from healthy, CD and UC patients was used as a source of PBMCs. PBMCs were pre-treated for 30 min with 1 μ M PPAR α/γ agonists prior to infection with *AIEC-LF82* (MOI 50) for 1h. PBMCs were subsequently treated with gentamicin to kill extracellular microbes for 60 min (~t0 h) prior to lysis and plating to determine the intracellular abundance of viable bacteria at t1h and t6h, as determined by dilution plating and colony counts (see Methods for details). Bar graphs with scatter plot display the abundance of viable intracellular bacteria at 1h (B) and 6h (E) after infection. Paired line plots display the rate of clearance of bacteria in individual subjects at 1h (C) and 6h (F) after infection. Data in B-C of 1h infection is combined in (D) and data from E and F 6h infection is combined in (G) with statistics: Results are displayed as mean \pm SEM (CD patient n=7, UC patients=6 and healthy n=9). Paired t-test or One-way ANOVA followed by Tukey's test for multiple comparisons was performed to test significance. Significance: ns: non-significant, *, p < 0.05; **, p < 0.01, ***, p < 0.001 and ****, p < 0.0001.

923
 924
 925
 926
 927
 928
 929
 930
 931
 932
 933
 934
 935
 936
 937
 938
 939
 940
 941
 942
 943
 944
 945
 946
 947
 948
 949
 950



951
952
953
954
955
956
957
958
959
960
961
962
963
964
965
966
967
968
969

Figure 7: Summary of findings and working model

Schematic summarizes key approaches and findings of this study. First, network-rationalized target identification (*Left*) was performed using web-based platform that queries > 1000 IBD datasets [⁹; see *Methods*] that served as 'input' to create a map of gene clusters that are progressively altered in the gut in the setting of IBD. Predictions are used to guide the choice of therapeutics (dual agonists of PPAR α and PPAR γ that have a balanced agonistic potential for both PPARs), the choice of animal models of IBD, predict cell types of action (macrophage processes), and finally, the subtype of IBD that could benefit most based on the cell type of action (i.e., CD). Second, experimentally determined mechanism of action studies (*right, top*) showed that balanced actions of both PPAR α and PPAR γ enable the induction of bacterial clearance, resolution of inflammation and healing; PPAR α is responsible for ROS and cytokine induction, whereas PPAR γ is responsible for anti-inflammatory response and healing. The dual agonistic action was superior to each agonist used alone. Third, targets validation studies (*right, bottom*) in murine and human models confirm the use of PPAR α/γ dual agonists for enhancing bacterial clearance and protection against colitis. When tested side-by-side in the infectious colitis model, the dual agonistic action was superior to each agonist used alone.

Figures

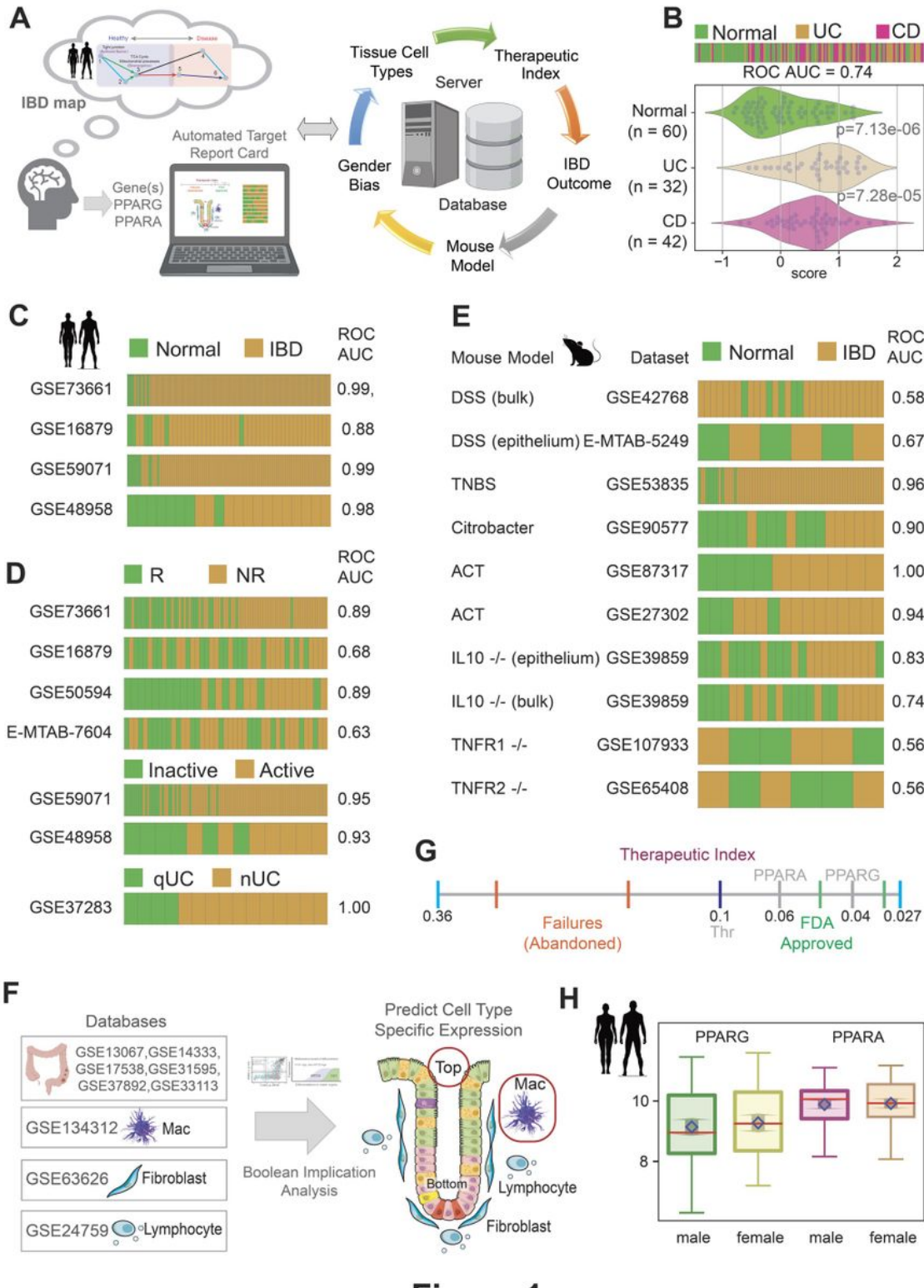


Figure 1

Network-rationalized target identification and study design. (A) Schematic displays the overall computationally guided study design. An interactive web-based platform allows the querying of paths of gene clusters in the IBD map [9; see Supplementary Fig. 1] to pick high-value targets with a few mouse

clicks and generate a comprehensive automated target 'report card'. The components of a 'target report card' is shown (right): predicted 'therapeutic index' (likelihood of Phase III success), IBD outcome (prognostic potential in UC and/or CD), network-prioritized mouse model, estimation of gender bias and predicted tissue cell type of action. (B-H) Components of a target report card for PPARA and PPARG are displayed. Bar plot (B; top) displays the rank ordering of normal vs ulcerative colitis (UC) /Crohn's Disease (CD) patient samples using the average gene expression patterns of the two genes: PPARG/PPARA. ROC-AUC statistics were measured for determining the classification strength of normal vs IBD. Bar plots (B; top) and violin plots (B; bottom) display the differences in the average expression of the two genes in normal, UC and CD samples in the test cohort used to build the IBD map. Bar plots in panel C-D show the rank ordering of either normal vs IBD samples (C) or responder vs non responder (R vs. NR; D), or active vs inactive disease, or neoplastic progression in quiescent UC (qUC vs. nUC; D) across numerous cohorts based on gene expression patterns of PPARG and PPARA, from high to low, left to right. Classification strength within each cohort is measured using ROC-AUC analyses. Bar plots in panel E show the rank ordering of either normal vs IBD samples across numerous published murine models of IBD based on gene expression patterns of PPARG and PPARA as in D. ACT = adoptive T cell transfer. Classification strength within each cohort is measured using ROC-AUC analyses. Bulk = whole distal colon; epithelium = sorted epithelial cells. Schematic in F summarizes the computational prediction of the cell type of action for potential PPARA/G targeted therapy, as determined using Boolean implication analysis. GSEID# of multiple publicly available databases of the different cell types and colorectal datasets used to make sure predictions are cited. Red boxes/circles denote that PPARA/G-targeted therapeutics are predicted to work on monocytes/macrophages and crypt-top enterocytes. Computationally generated therapeutic index (see Methods) is represented as a line graph in G. The annotated numbers represent Boolean implication statistics. PPARA and PPARG align with FDA approved targets on the right of threshold (0.1). Two FDA approved targets (green; ITGB1, 0.046; JAK2, 0.032), two abandoned targets (red; SMAD7, 0.33; IL11, 0.16), PPARA (grey, 0.064), PPARG (grey, 0.04), and the threshold (black, 0.1) are shown in the scale. Box plot in panel H shows that the level of PPARA/G expression is similar in the colons of both genders in health and in IBD, and hence, PPARA/g-targeted therapeutics are predicted to have little/no gender predilection.

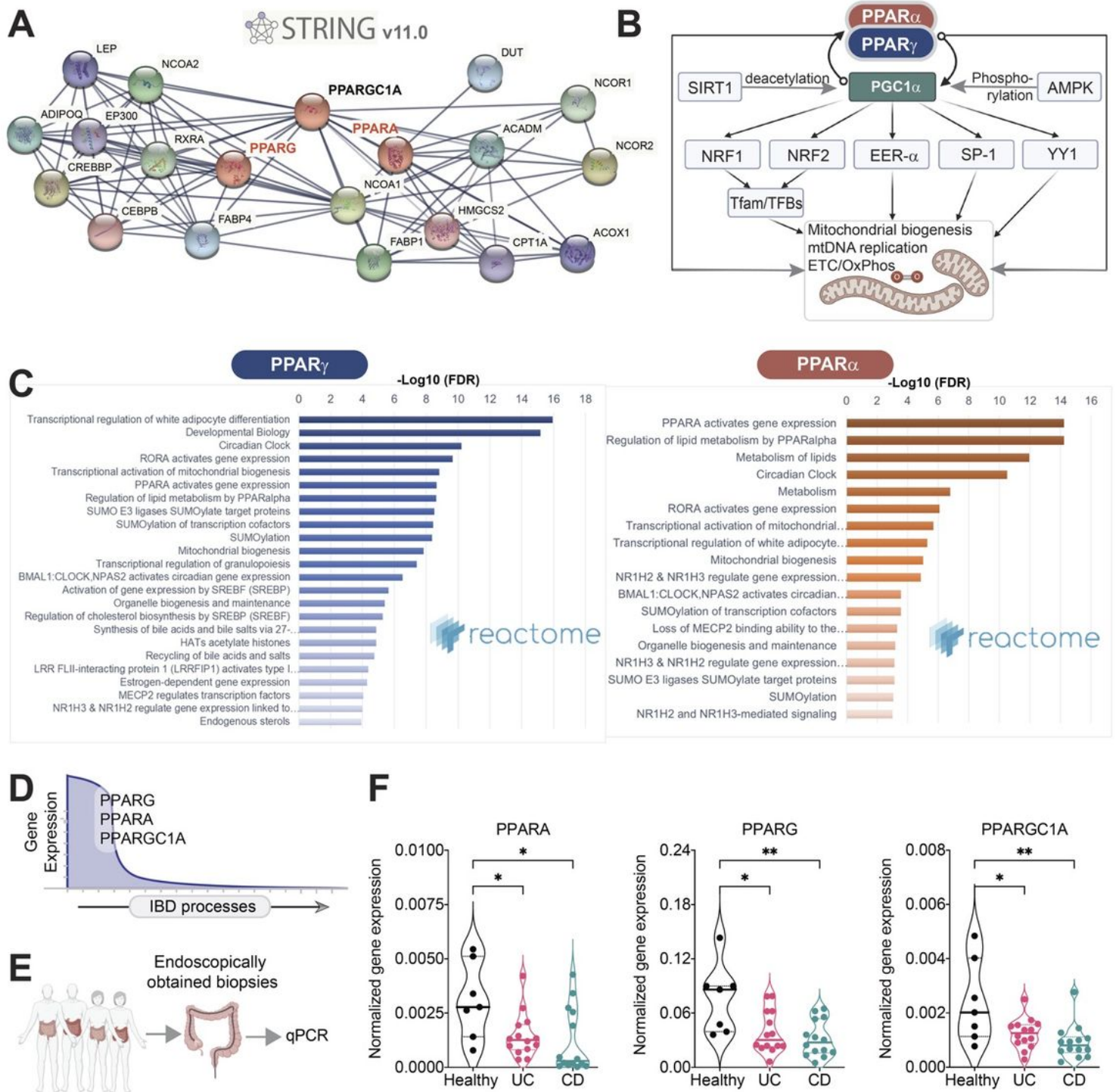


Figure 2

Rationalization of PPAR α and PPAR γ as targets in IBD. (A) A protein-protein interaction network (i.e., interactomes) for PPAR α and PPAR γ , generated using STRING v.11 (<https://string-db.org>). (B) Schematic summarizing the roles of PPAR α , PPAR γ and PGC1 α on mitochondria biogenesis and function (based on). PGC1- α emerges as a critical hub for forward feedback loops. (C) Reactome pathway analyses (www.reactome.org) on PPAR- α and PPAR- γ interactomes in A show convergence on metabolism,

mitochondria bioenergetics and the circadian clock. (D) Graphical visualization of the predicted changes in the expression of PPARA (PPAR- α), PPARG (PPAR- γ) and PPARGC1A (PGC1- α) genes during the progression of IBD processes (indicated with an arrow). (E) Schematic showing validation workflow; the expression of PPARA, PPARG and PPARGC1A transcript levels were assessed in the ileum/colon biopsies of IBD patients (UC=14 and CD= 14) or healthy controls (n=7). (F) Violin plots display the qPCR results in E. Results are displayed as mean \pm SEM. Significance was tested using one-way ANOVA followed by Tukey's test for multiple comparisons. Significance: *, $p < 0.05$; **, $p < 0.01$.

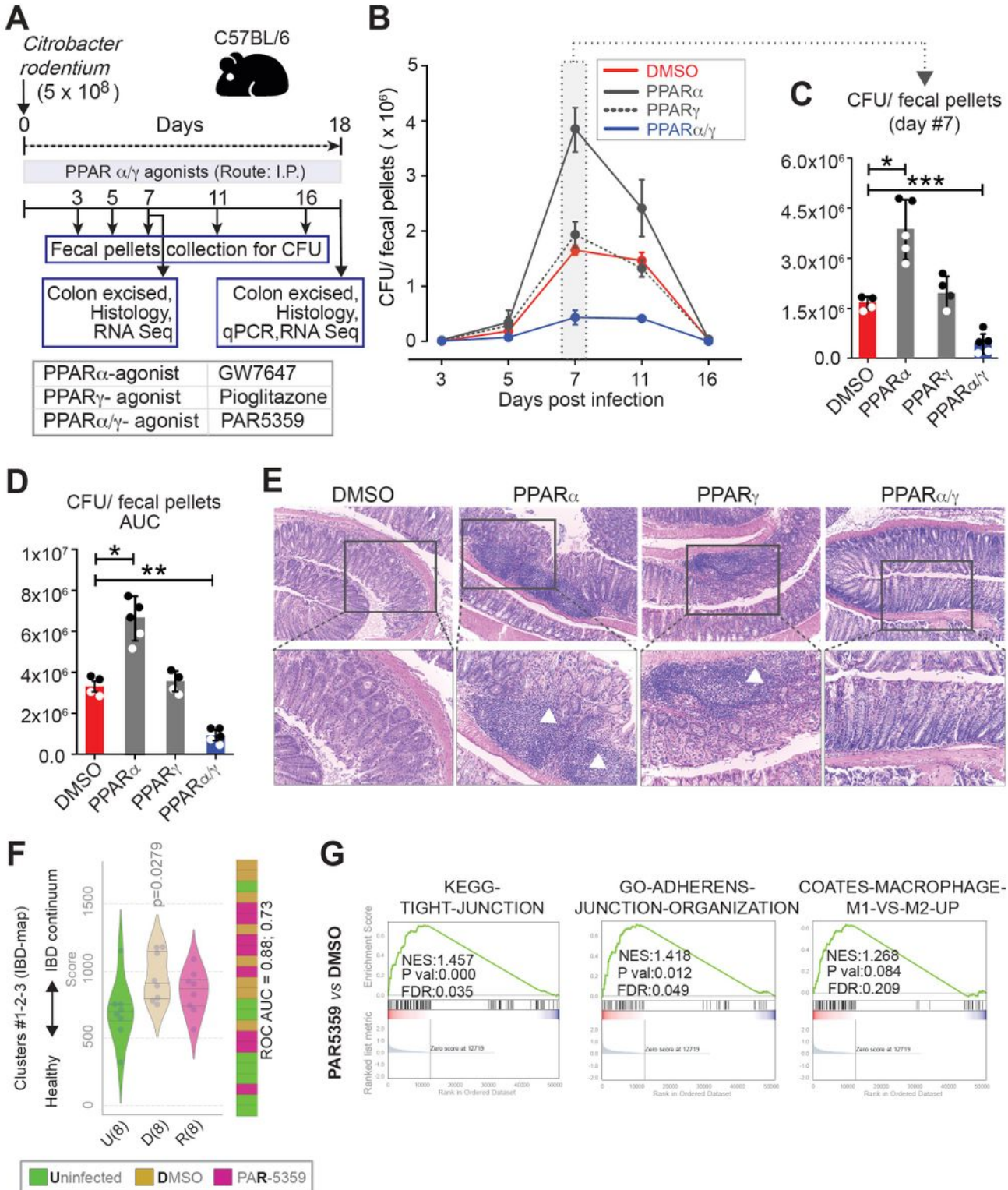


Figure 3

PPAR α / δ dual agonists ameliorate *Citrobacter rodentium*-induced infectious colitis in mice. (A) Schematic summarizing the workflow for testing PPAR-targeted therapeutics in *C. rodentium*-induced colitis. Mice were gavaged with *C. rodentium* on day 0 and subsequently treated daily with PPAR agonists. Fecal pellets were collected to test viable bacterial burden, as determined by dilution plating and colony counting. Colons were excised on day 7 and 18 and analyzed using the indicated readouts. (B-D) Line graphs in B display time series of the burden of viable bacteria in feces. Scatter plots with bar graphs in C compare the peak burden of viable bacteria in feces on day 7. Scatter plots with bar graphs in D display the area under the curve (AUC) for the line graph in B. (E) Images display representative fields from H&E-stained colon tissues. Mag = 100x (top) and 200x (bottom). White arrowheads point to immune cell infiltrates. Statistics: All results are displayed as mean \pm SEM. Significance was tested using two-way/one-way ANOVA followed by Tukey's test for multiple comparisons. Significance: *, $p < 0.05$; **, $p < 0.01$, ***, $p < 0.001$. (F) Violin plots (left) display the deviation of expression of genes in Clusters #1-2-3 in the IBD network, as determined by RNA Seq on murine colons. Bar plot (right) displays the rank ordering of the samples. (G) Pre-ranked GSEA based on pairwise differential expression analyses (DMSO vs PAR5359 groups) are displayed as enrichment plots for epithelial tight (left) and adherens (middle) junction signatures and balanced macrophage processes (right). See also Supplementary Fig. 7 for the Day #7 results in the *C. rodentium*-induced colitis model, Supplementary Fig. 8 for extended GSEA analyses, and Supplementary Fig. 9 for the effect of PAR5359 on DSS-induced colitis in mice.

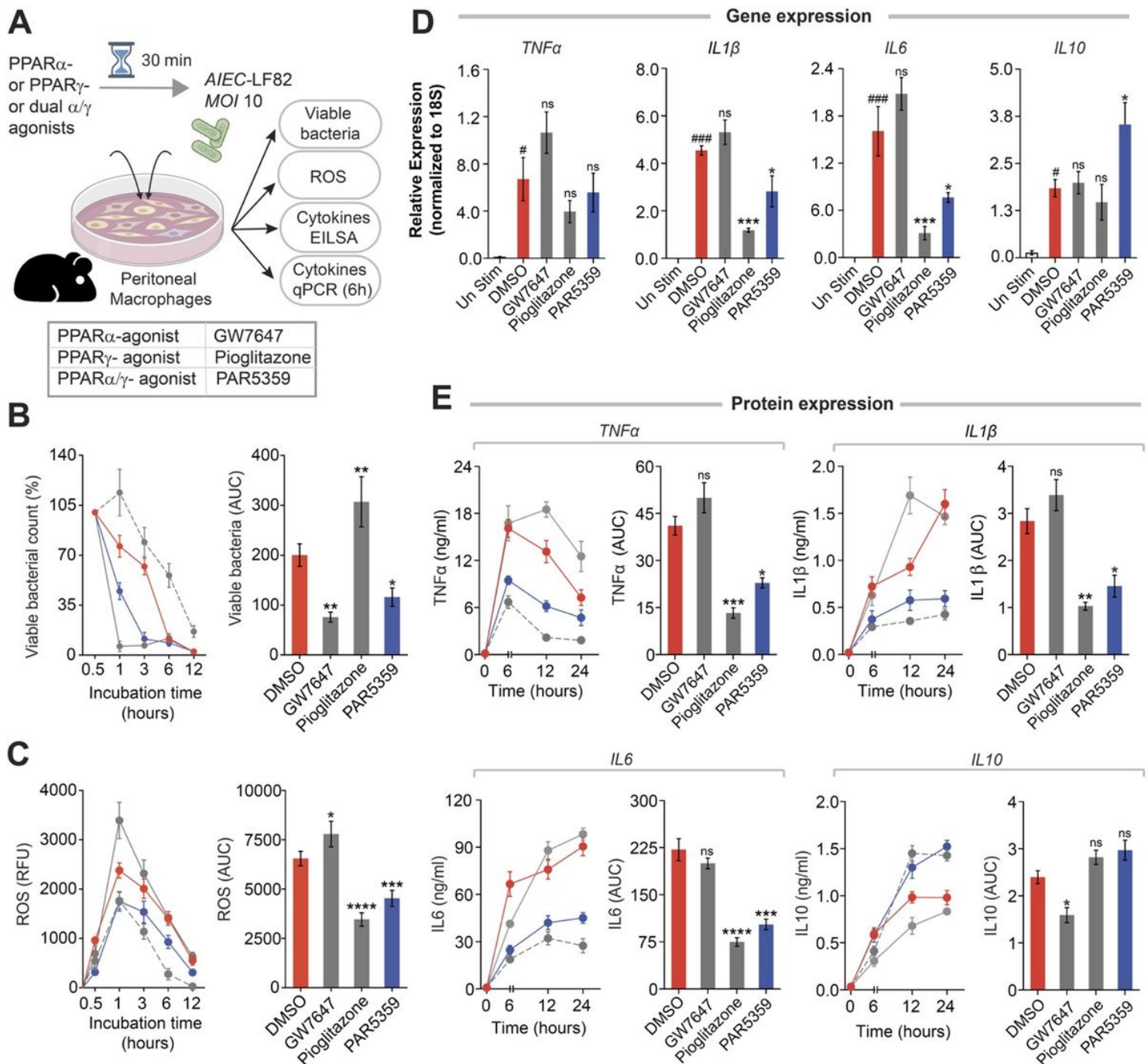


Figure 4

PPAR α and PPAR α/γ -dual agonists enhance, whereas PPAR γ agonist delay bacterial (AIEC LF82) clearance. (A) Schematic displays the experimental design and workflow. Thioglycolate-induced murine peritoneal macrophages (TG-PM) pretreated with PPAR agonists (see box, below; 20 nM GW7647, 10 μ M Pioglitazone and 1 μ M PAR5359) were infected with AIEC-LF82 (MOI 10) and subsequently analyzed for the bacterial count (Gentamycin protection assay), generation of cellular ROS, secretion of inflammatory cytokines (in supernatant media by ELISA) and the induction of cytokines (gene transcript analysis by qPCR). (B) Line graphs (left) display percent viable bacterial counts at indicated times after infection. Bar graphs (right) display the AUC. (C) Line graphs (left) and bar graphs (right) display the

extent of ROS generation over time. (D) Bar graphs display the relative expression of transcripts of multiple cytokines (IL1 β , IL6, TNF α and IL10). (E) Line graphs (left) and bar graphs (right) showing the levels of secreted cytokines in the media. Statistics: All results are from at least three independent experiments and results displayed as means \pm SEM. Significance was tested using two-way/one-way ANOVA followed by Tukey's test for multiple comparisons. Significance: '#' significance over uninfected TG-PMs and '*' shows significance over AIEC-LF82 infected cells. ns, nonsignificant, *, $p < 0.05$; **, $p < 0.01$, ***, $p < 0.001$, ****, $p < 0.0001$. See Supplementary Fig. 10 for similar bacterial clearance assays performed using *Salmonella enteritica*.

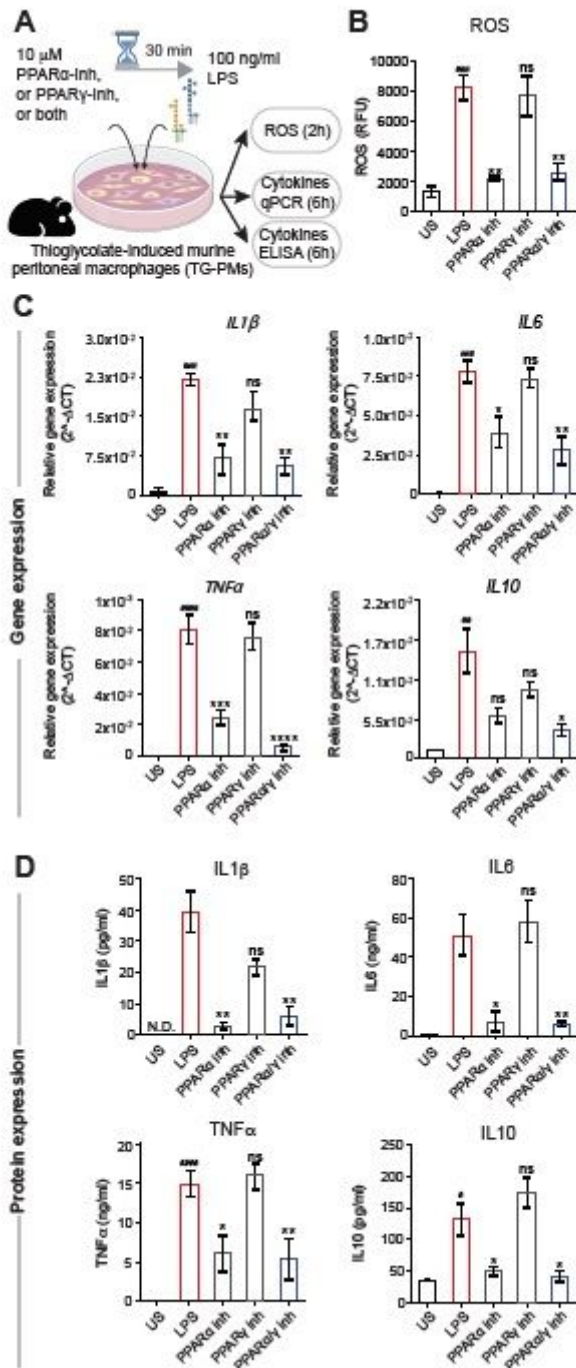


Figure 5

PPAR α but not PPAR γ is required for induction of cellular ROS and proinflammatory cytokines. (A) Schematic of experimental design. TG-PMs were pre-incubated with 10 μ M PPAR α or PPAR γ inhibitors, either alone or in combination for 30 min prior to stimulation with 100 ng/ml LPS. Cells were analyzed at 2 and 6 h to estimate cellular ROS and cytokine induction, respectively. (B-D) Bar graphs display the levels of cellular ROS (B), relative levels of mRNA (C) and protein (D) expression of cytokines (IL1 β , IL6, TNF α and IL10). Statistics: Results are from three independent experiments and displayed as mean \pm SEM. One-way ANOVA followed by Tukey's test for multiple comparisons was performed to test significance. Significance: ns: nonsignificant, *, $p < 0.05$; **, $p < 0.01$, ***, $p < 0.001$ and ****, $p < 0.0001$.

PPAR α but not PPAR γ is required for induction of cellular ROS and proinflammatory cytokines. (A) Schematic of experimental design. TG-PMs were pre-incubated with 10 μ M PPAR α or PPAR γ inhibitors, either alone or in combination for 30 min prior to stimulation with 100 ng/ml LPS. Cells were analyzed at 2 and 6 h to estimate cellular ROS and cytokine induction, respectively. (B-D) Bar graphs display the levels of cellular ROS (B), relative levels of mRNA (C) and protein (D) expression of cytokines (IL1 β , IL6, TNF α and IL10). Statistics: Results are from three independent experiments and displayed as mean \pm SEM. One-way ANOVA followed by Tukey's test for multiple comparisons was performed to test significance. Significance: ns: nonsignificant, *, $p < 0.05$; **, $p < 0.01$, ***, $p < 0.001$ and ****, $p < 0.0001$.

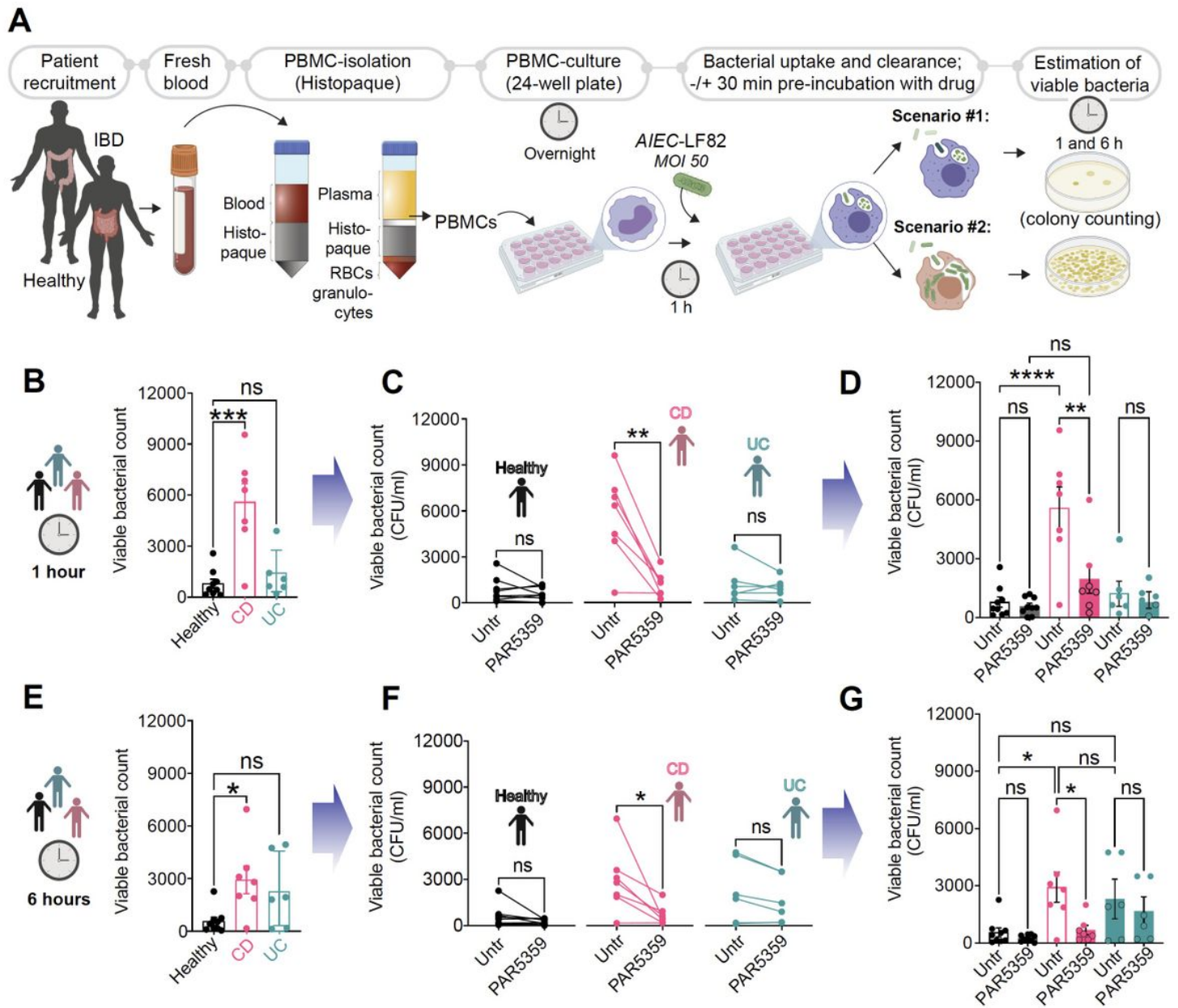


Figure 6

PPAR α /g dual agonist, PAR5359, promotes the clearance of AIEC-LF82 from CD patient-derived PBMCs. (A) Schematic displays the overall experimental design using human subjects (see Table 5 for patient demographics). Peripheral blood collected from healthy, CD and UC patients was used as a source of PBMCs. PBMCs were pre-treated for 30 min with 1 μ M PPAR α /g agonists prior to infection with AIEC-LF82 (MOI 50) for 1h. PBMCs were subsequently treated with gentamicin to kill extracellular microbes for 60 min (~t₀ h) prior to lysis and plating to determine the intracellular abundance of viable bacteria at t₁h and t₆h, as determined by dilution plating and colony counts (see Methods for details). Bar graphs with scatter plot display the abundance of viable intracellular bacteria at 1h (B) and 6h (E) after infection. Paired line plots display the rate of clearance of bacteria in individual subjects at 1h (C) and 6 h (F) after infection. Data in B-C of 1h infection is combined in (D) and data from E and F 6h infection is combined in (G) with statistics: Results are displayed as mean \pm SEM (CD patient n=7, UC

patients=6 and healthy n=9). Paired t-test or One-way ANOVA followed by Tukey's test for multiple comparisons was performed to test significance. Significance: ns: non-significant, *, $p < 0.05$; **, $p < 0.01$, ***, $p < 0.001$ and ****, $p < 0.0001$.

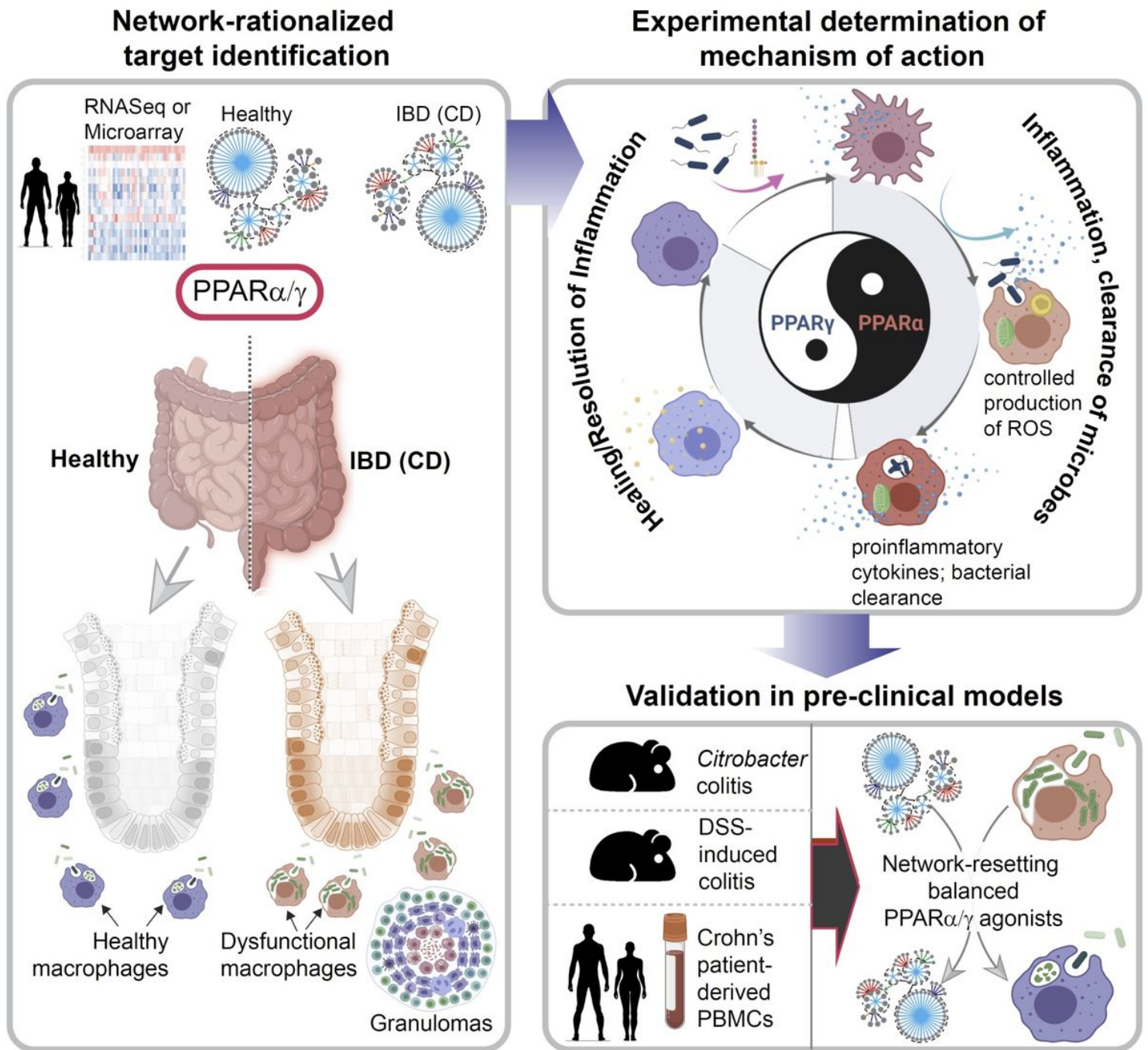


Figure 7

Summary of findings and working model Schematic summarizes key approaches and findings of this study. First, network-rationalized target identification (Left) was performed using web-based platform that queries > 1000 IBD datasets [9; see Methods] that served as 'input' to create a map of gene clusters that are progressively altered in the gut in the setting of IBD. Predictions are used to guide the choice of therapeutics (dual agonists of $PPAR\alpha$ and $PPAR\gamma$ that have a balanced agonistic potential for both

PPARs), the choice of animal models of IBD, predict cell types of action (macrophage processes), and finally, the subtype of IBD that could benefit most based on the cell type of action (i.e., CD). Second, experimentally determined mechanism of action studies (right, top) showed that balanced actions of both PPAR α and PPAR γ enable the induction of bacterial clearance, resolution of inflammation and healing; PPAR α is responsible for ROS and cytokine induction, whereas PPAR γ is responsible for anti-inflammatory response and healing. The dual agonistic action was superior to each agonist used alone. Third, targets validation studies (right, bottom) in murine and human models confirm the use of PPAR α / γ dual agonists for enhancing bacterial clearance and protection against colitis. When tested side-by-side in the infectious colitis model, the dual agonistic action was superior to each agonist used alone.

Supplementary Files

This is a list of supplementary files associated with this preprint. Click to download.

- [nrreportingsummaryFILLED.pdf](#)
- [2.Supplementaryonlinematerials.pdf](#)